Geoderma 226–227 (2014) 300–316

Contents lists available at ScienceDirect

Geoderma

journal homepage: www.elsevier.com/locate/geoderma

Pedogenesis, permafrost, substrate and topography: Plot and landscape scale interrelations of weathering processes on the central-eastern Tibetan Plateau

Frank Baumann [a,*], Karsten Schmidt [a], Corina Dörfer [a], Jin-Sheng He [b], Thomas Scholten [a], Peter Kühn [a]

[a] Department of Geosciences, Chair of Physical Geography and Soil Science, Eberhard Karls Universität Tübingen, Ruemelinstrasse 19-23, 72070 Tuebingen, Germany
[b] Department of Ecology, College of Urban and Environmental Sciences, Peking University, 100871 Beijing, China

ARTICLE INFO

Article history:
Received 20 September 2013
Received in revised form 16 February 2014
Accepted 23 February 2014
Available online 17 March 2014

Keywords:
Tibetan Plateau
Pedogenesis
Permafrost
Weathering indices
Pedogenic oxides
Multiple linear regression

ABSTRACT

Weathering indices (WI) and pedogenic oxides ratios (POR) were used to describe patterns of weathering intensities and pedogenesis along climatic gradients, mainly affected by varying influences of the Asian and Indian Monsoon. These climate settings induce particular soil moisture (SM) conditions, in turn closely related to permafrost state, substrate, and topography. Nine sites including a total of 30 soil profiles were examined along an eastern and a western transect across the central-eastern Qinghai–Tibet Plateau. Additionally, differences between four soil groups were analysed. According to our knowledge, the presented study is the first attempt of a comprehensive application of different WI and POR to substrates of currently permafrost-affected soils. It provides an evaluation of various tools in terms of chemically describing and differentiating the related processes to distinct environmental settings in low-weathering regions. We found that weathering trends along the climatic gradients could be clearly outlined by WI, whereas POR rather account for small scale variations, describing significant differences of pedogenesis between continuous and discontinuous permafrost conditions. Pyrophosphate soluble iron (Fep) proved to be useful for differentiating permafrost and ground water influenced soils, showing a strong correlation to total organic carbon ($r = 0.89$). The chemical index of alteration (CIA) is the most suitable WI, whereas Ca-free CPA is more easily biased by salinity variations of topsoils at sites with negative water balance, thus pretending lower weathering intensities. Regression analyses for WI and POR with main independent variables underline the specific characteristics: climatic parameters best explain WI, while SM is dominant for POR. The ratio (Fed-Feo)/Fet proved as the most appropriate POR with 64% explained variation by a multiple linear regression model, implying significantly lower iron release with higher SM and pH values. Variation of Fep can be explained by 63% with soil acidity being most important, followed by SM. Importantly, the presented research provides tools for investigating past and future stability or respective degradation processes of permafrost ecosystems on the Tibetan Plateau and may be applicable to other permafrost-affected environments.
© 2014 Elsevier B.V. All rights reserved.

1. Introduction

Pedogenesis and the state of soil development are considered to be important predictors for total soil organic carbon (TOC) and nitrogen contents of permafrost-affected soils on the Tibetan Plateau (Baumann et al., 2009). Soil development is closely associated with specific weathering intensities under distinct environmental conditions (Brady and Weil, 2008; Jenny, 1994). Hence, the presented research provides an approach to evaluate and differentiate pedogenesis by soil chemical properties in relation to their main influencing factors.

Chemical weathering processes release iron and other elements contained in primary minerals of bedrocks and sediments. Depending on various soil characteristics, such as soil moisture (SM), soil temperature (ST), soil acidity, and redox conditions, distinct pedogenic oxides (PO) are formed under a particular timeframe (Kämpf et al., 2011). By extracting fractions of PO with specific degrees of crystallisation, it is possible to determine intensity, duration, quality, and direction of pedogenic processes (McKeague, 1967; Mehra and Jackson, 1960; Schlichting and Blume, 1962; Schwertmann, 1964). Several pedogenic oxides ratios (POR) have been successfully applied to describe and relatively date geomorphological units (e.g. Aniku and Singer, 1990; Arduino et al., 1984; Mirabella and Carnicelli, 1992; Torrent et al., 1980) as well as soil weathering

Abbreviations: WI, weathering indices; PI, Parker index; KN, Kronberg & Nesbitt Index; CIA, chemical index of alteration; CIW, chemical index of weathering; PIA, plagioclase index of alteration; CPA, chemical proxy of alteration; PO, pedogenic oxides; POR, pedogenic oxides ratios; MAT, mean annual air temperature; MAP, mean annual precipitation; SM, soil moisture; ST, soil temperature; TOC, total soil organic carbon; SG, soil group; RG, Regosols; CM, Cambisols; GL, Gleysols; PF, permafrost-affected soils.

* Corresponding author. Tel.: +49 7071 29 74896; fax: +49 7071 29 5391.
E-mail address: frank.baumann@uni-tuebingen.de (F. Baumann).

http://dx.doi.org/10.1016/j.geoderma.2014.02.019
0016-7061/© 2014 Elsevier B.V. All rights reserved.

chronosequences and palaeosols (e.g. Buero and Schwertmann, 1987; Dahms et al., 2012; Diaz, 1989; Mahaney and Fahey, 1980; McFadden and Hendricks, 1985; Rezapour et al., 2010; Sauer et al., 2010; Torrent et al., 2007). However, only few soil surveys systematically investigated PO in periglacial environments and under the scope of current soil formation (Melke, 2007).

Weathering indices (WI) have been primarily developed for sedimentary geology (e.g. Cullers, 2000; McLennan, 1993; Yang et al., 2004). Many studies have adopted these tools for analysing and describing geomorphological units, loess layers and palaeosols (e.g. Bäumler, 2001; Bäumler and Zech, 2000; Buggle et al., 2008, 2011; Gallet et al., 1998; Kühn et al., 2013; Wagner, 2005). Weathering intensities have been investigated in arctic permafrost and glaciated areas (Bäumler, 2001; Melke, 2007; Wagner, 2005), whereas only little research has been done in dry permafrost areas like the Tibetan Plateau. Due to the cold and arid climate, low chemical weathering intensities are expected in periglacial environments (Brady and Weil, 2008; Fedo et al., 1995; McLennan, 1993).

The Tibetan Plateau extends over more than 2.4 million km^2 on an average altitude of 4000 m a.s.l., representing the largest high-altitude and low-latitude permafrost area on earth. It proved to be particularly sensitive in terms of global warming (Qiu, 2008) and land use changes (Yang et al., 2009). About 54% of the plateau's surface is directly influenced by permafrost (Cheng, 2005). Over the past decades, permafrost degradation processes can be more frequently observed with corresponding changes in soil moisture–temperature regimes (e.g. Cheng and Wu, 2007; Jin et al., 2000; Kang et al., 2010; Yang et al., 2010, 2011; Zhang et al., 2003) and desertification processes (Wang et al., 2011; Xue et al., 2009; Yan et al., 2009). Soil's properties are accordingly altered, reassigning their role in ecosystem functioning (Chapin et al., 2000; Vitousek, 1997). This leads to instability and erosional features mainly triggered by widespread occurring loose sediments and sparse vegetation, which in turn is a result of lower soil moisture contents as a consequence of permafrost degradation (Baumann et al., 2009). Consequently, decreasing soil organic carbon contents can be observed (Dai et al., 2011).

Distinct climate gradients are evident across the research area (An et al., 2001), exhibiting clearly differing mean annual air temperature (MAT) and mean annual precipitation (MAP) as independent variables for soil weathering. Together with the above-described prerequisites and processes, the altering permafrost-affected ecosystems on the Tibetan Plateau provide an ideal compound to examine the use of POR and WI to describe weathering processes on both landscape scale and plot scale. In accordance to our present knowledge, this is the first study systematically analysing interdependencies of PO and WI in substrates subjected to current soil formation in permafrost environments across climate transects.

The primary objective of this study is to investigate the influence of permafrost on weathering intensity and pedogenesis. We hypothesise that:

(1) SM is a key variable for pedogenesis and weathering processes, mainly determined by permafrost characteristics, substrate, and topography.
(2) SM content is interrelated to distinct precipitation–temperature ratios and thus to specific permafrost distribution, caused by varying influences of monsoon systems between the eastern and western transect as well as along each transect.
(3) Intensity of weathering and pedogenesis can be described by WI, PO fractions and POR. These indicators are in turn all essentially related to independent moisture parameters showing clear differences along climate transects and specifically between continuous and discontinuous permafrost. By consideration of other independent parameters, WI and POR can be evaluated with regard to their validity in comparable environments.

2. Materials and methods

2.1. Environmental settings

Data presented in this paper were gathered during field work on the central-eastern Tibetan Plateau in the years 2006, 2007 and 2009 along an eastern and western transect, which both are north–south oriented (Fig. 1, Table 1). Sites on the eastern transect (EAST) extend along 98.5°E and range from 34.3 to 35.3°N in the region between the settlements of Huashixia and Yushu, whereas the western transect (WEST) stretches along 92.2°E and ranges from 31.4 to 34.7°N between Wudaoliang and Nagqu.

MAT ranges from −3.5 to −5.7 °C on the eastern transect and from −0.2 to −5.6 °C on the western transect. Mean annual precipitation (MAP) varies from 458 to 521 mm (EAST) and 285 to 510 mm (WEST) with 80% of the rainfall occurring during the summer months. Thus, two major climatic trends are evident in the research area: the subtropical East Asian Monsoon transporting comparably warm and moist air from the eastern lowlands to the eastern Tibetan Plateau during summer months decreasing westwards, and the Tropical Indian Monsoon influencing the Tibetan Plateau from the south (Domrös and Peng, 1988). The east–west oriented mountain ranges are important barriers for these airmasses. During the cold and dry winters, extratropical westerlies occur together with the prevailing Mongolian–Siberian high pressure system. Temperature and precipitation generally decreases from SE to NW, locally strongly influenced by topography and elevation. This explains the differences between sites E1 and E2 of EAST: they are geographically located next to each other but have pronounced climatic differences, which is caused by the Anyêmaqên Mountain Range located in the east. Site E2 is in lee position, showing lower rainfall with higher temperatures compared to E1, where an east–west stretching furrow between the Anyêmaqên and Bayan Har Mountains locally leads to higher rainfall and lower temperatures. Site E3 is located southwards close to Bayan Har pass, explaining the lower MAT and higher MAP. Similar situations occur in WEST, with the Tanggula Mountains being the most eminent climatic divide. Evaporation ranges on average for the whole Tibetan Plateau between 1204 and 1327 mm (Wang and French, 1994), reaching 1478 mm in the headwaters of Yangtze River (Hu et al., 2009), 1264 mm in the headwaters of Yellow River around Maduo (Zhang et al., 2010) and 1770 mm in the area around Amduo (Feng and Zhu, 2009). Gao et al. (2006) provide evaporation values ranging from 1500 to 2300 mm for Nagqu County rising from SE to NW. Hence, evaporation far exceeds precipitation in the whole research area.

Permafrost characteristics and distribution are closely linked to climatic patterns (Ping et al., 2004; Wang and French, 1994, Fig. 1). Active layer thickness averages around 1–2 m, increasing from northwest to southeast and with decreasing altitude (Cheng and Wu, 2007; Wang et al., 2000). EAST is characterised by discontinuous and unstable permafrost conditions with a widespread vertical disconnection in the area around Huashixia. In these cases, soils freeze seasonally to a depth of 2–3 m with the upper limit of permafrost located in 4–7 m depth (Jin et al., 2000). This vertical freezing-gap is non-existent with higher elevation, as can be observed for the Bayan Har Shan site (E3). The western transect extends from continuous ice-poor permafrost in the area around Wudaoliang (W1/W2), to sporadic island permafrost in the region around Nagqu (W6/W7). Permafrost degradation, also caused by former construction activities, lead to the formation of numerous small depressions, where surface water accumulates or thermokarst lakes are formed (Niu et al., 2011). Moreover, desertification is a major consequence of permafrost degradation frequently observable in the research area (Xue et al., 2009).

Glacial aeolian loess-like sediments and sediments dominated by silt and fine sand fractions, being mainly of local origin (Feng et al., 2011), cover most slopes and terraces providing the main parent material for pedogenesis (Schlütz and Lehmkuhl, 2009). Soil formation is closely

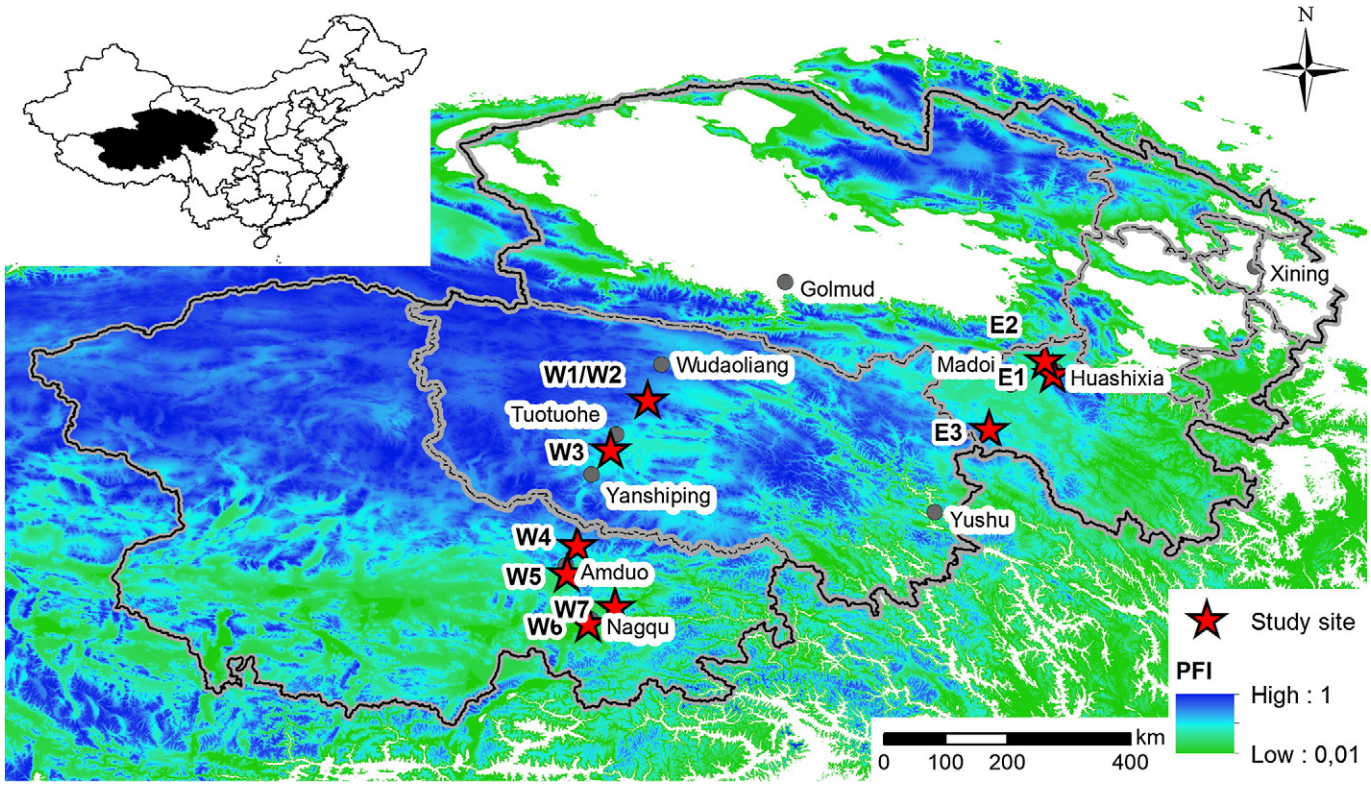

Fig. 1. Study sites split into transect EAST (E1–E3) and WEST (W1–W7). Permafrost distribution is displayed by Permafrost Zonation Index (PFI) (Gruber, 2012).

related to permafrost conditions and topography (Baumann et al., 2009). It is subjected to broad ranges of substrates and geomorphological processes, frequently interrupted by fresh, mainly aeolian sedimentation and cryogenic (solifluction) or erosive processes. This often leads to buried, mainly humic horizons. Only weakly developed and frequently polygenetic formed soils on slopes and terraces (Leptosols, Leptic Cambisols, Haplic Regosols, Mollic Cryosols), as well as Gleysols and Gelic Gleysols occur in depressions next to rivers or lakes (Kaiser, 2004; Kaiser et al., 2007). This instability is enhanced by intense precipitation during the summer months leading to fluvial erosion and alluvial accumulation also by laminar sheet floods along gentle slopes (cf. site E2), whereas aeolian erosion and re-deposition is forced in such areas during winter triggered by the dry winter monsoon and sparse vegetation (Dietze et al., 2012; Xue et al., 2009). Under more stable conditions (cf. site W1/W2), Cambic Cryosols and well-developed Cambisols are evident, mirroring specific permafrost and climate conditions. The most widespread vegetation types are alpine *Kobresia* meadow and alpine steppe. Particularly in alpine meadow ecosystems, felty topsoils with a high root density are common (Kaiser et al., 2008).

2.2. Field methods

The sampling sets can be generally divided into an eastern (EAST) and western (WEST) transect (Fig. 1). Along each transect main sites and support sites were established. Main sites consist of several soil profiles, arranged along soil catenas, while support sites usually comprise only one soil profile (Table 1). Thus, both the variation within sites and along transects is represented. Although the climate gradient is stretching from SE to NW, the parallel N–S oriented transects provide the opportunity to study the distinct monsoonal influences. Each soil profile was described according to FAO (2006) and IUSS Working Group WRB (2006). Soil sampling was split into three parts: horizon-wise sampling to determine all relevant parameters for description of weathering and pedogenesis using soil pits; schematic sampling by drilling at three depth-increments (0–5, 5–10, and 10–20 cm) for C and N analysis and basic soil parameters as interpolation points between soil pits in catenas; volumetric samples at equal depths for bulk density and gravimetric water content determination. SM was additionally determined directly in the field by TDR-probes (Delta-T Devices Ltd., Cambridge, UK) for all pedogenic horizons as well as for depth increments.

Table 1
Physiographic environment and main soil groups of the main study sites in the central-eastern Tibetan Plateau. For detailed information on all sampled soil profiles and horizons including the complete parameter set see electronic Supplementary data S1.

Location	Transect	Site name	Altitude [m asl]	MAT [°C]	MAP [mm]	Soil group	No. profiles
Huashixia	East	E1	4310	−4.6	493	RG, GL, PF	6
Donggi Cona	East	E2	4095	−3.5	458	RG, CM, GL	4
Yushu	East	E3	4667	−5.7	522	PF	1
Wudaoliang West	West	W1	4804	−5.6	307	CM, GL, PF	5
Wudaoliang East	West	W2	4753	−5.2	285	PF	2
Tuotuohe	West	W3	4654	−4.2	336	RG	1
Tanggula	West	W4	5105	−5.8	489	PF	1
Amduo	West	W5	4903	−4.2	473	CM, PF	2
Nagqu West	West	W6	4494	−0.3	480	CM, GL	7
Nagqu East	West	W7	4596	−1.9	511	PF	1

2.3. Laboratory analyses

All soil samples were air-dried and sieved to <2 mm. Grain size analysis was conducted by combined pipette and sieving method (7 fractions, Koehn, DIN 19683–1). Electrical conductivity (EC) was measured in bi-distilled H_2O, whereas pH was determined in 0.01 M $CaCl_2$ potentiometrically. $CaCO_3$ was analysed gas-volumetrically on ground subsamples. Total organic carbon (TOC) was measured with heat combustion (VARIO EL III, Elementar, Hanau, Germany). C bound in $CaCO_3$ was subtracted from the total amount of C (TC) quantified with the CNS analyser to obtain the proportion of organic C (TOC). Water content was quantified gravimetrically and corrected by the skeleton content (>2 mm).

Total element contents were determined by X-ray fluorescence. The results constitute the basis for the calculation of weathering indices and the determination of Fet. Pedogenic Fe-oxides (Fed) were extracted by dithionite–citrate–bicarbonate (DCB) solution (Mehra and Jackson, 1960); non crystallised and poorly crystallised Fe-oxides, hydroxides and associated gels (Feo) were extracted by acid ammonium oxalate solution (Schwertmann, 1964); and Fe-oxides and metalorganic compounds mainly bound in organic matter (Fep) by 0.1 M pyrophosphate solution (Bascomb, 1968; McKeague, 1967). All extractions were analysed with inductively coupled plasma optical emission spectrometry (ICP-OES), using Optima 5300 DV, PerkinElmer, Waltham, USA.

2.4. Weathering indices

The following weathering indices (WI) were calculated and compared. Parker Index (PI) calculates on atomic proportions; all other WI on molar proportions of the total elemental contents.

$$\text{Parker index (PI)}: \mathrm{PI} = (\mathrm{Na_a}/0.35 + \mathrm{Mg_a}/0.9 + \mathrm{K_a}/0.25 + \mathrm{Ca_a}/0.7) \times 100; \quad (1)$$

where X_a = % element X/atomic weight of X.

PI calculates the amount of alkali and alkaline earth cations lost and subsequently leached by mineral hydrolysis. The strength of the element–oxygen bond in the primary minerals element contents are considered by weighting the element contents by a corresponding factor (Bäumler, 2001). This factor is resulting from Nicholls' values of bond strength which accounts for the probability of an element to get mobilised (Parker, 1970).

The PI's major drawback is not to consider comparably immobile reference phases, such as Al_2O_3 for measuring relative shifts of composition of relevant mineral components. Moreover, it is assumed that all Ca is contributed by silicate minerals leading to inaccuracies, if larger carbonate contents are evident. The index decreases with weathering intensity and soil development.

$$\begin{aligned}&\text{Kronberg \& Nesbitt index (KN)(Kronberg and Nesbitt, 1981)}:\\ &\text{Index A} = (\mathrm{SiO_2} + \mathrm{CaO} + \mathrm{K_2O} + \mathrm{Na_2O})/(\mathrm{Al_2O_2} + \mathrm{SiO_2} + \mathrm{CaO} + \mathrm{K_2O} + \mathrm{Na_2O}) \quad (2)\\ &\text{Index B} = (\mathrm{CaO} + \mathrm{K_2O} + \mathrm{Na_2O})/(\mathrm{Al_2O_3} + \mathrm{CaO} + \mathrm{K_2O} + \mathrm{Na_2O})\end{aligned}$$

Index A (abscissa) accounts for the relative enrichment of Al and Si oxide phases and inversely measures the leaching of Na, K and Ca. The selective accumulation of Al and Si provides information, if chemical weathering (Al enrichment; index calculates against 0) or physical weathering (Si enrichment; index calculates against 1) is prevailing.

Index B (ordinate) evaluates the degree of feldspar breakdown indicating the alteration of feldspar and formation of clay minerals. Consequently, the index also decreases with increasing weathering intensity. The main disadvantage of this index as well as for the PI is that CaO is not corrected for the carbonate content.

$$\text{Weathering index for carbonate-rich sediments (Feng, 1997)}: \mathrm{FENG} = (\mathrm{Al_2O_3} + \mathrm{Fe_2O_3})/(\mathrm{Na_2O} + \mathrm{K_2O} + \mathrm{MgO} + \mathrm{P_2O_5}) \quad (3)$$

Feng (1997) factored out Ca to avoid the above-described biases of carbonate and included instead Mg and P as critical determinants. This index increases during soil development and weathering processes.

$$\text{Chemical index of alteration (CIA)(Nesbitt and Young, 1982)}: \mathrm{CIA} = \left[\mathrm{Al_2O_3}/(\mathrm{Al_2O_3} + \mathrm{Na_2O} + \mathrm{CaO^*} + \mathrm{K_2O})\right] \times 100 \quad (4)$$

$$\text{Chemical index of weathering (CIW)(Harnois, 1988)}: \mathrm{CIW} = \left[\mathrm{Al_2O_3}/(\mathrm{Al_2O_3} + \mathrm{Na_2O} + \mathrm{CaO^*})\right] \times 100 \quad (5)$$

$$\text{Plagioclase index of alteration (PIA)(Fedo et al., 1995)}: \mathrm{PIA} = \left[(\mathrm{Al_2O_3} - \mathrm{K_2O})/(\mathrm{Al_2O_3} + \mathrm{CaO^*} + \mathrm{Na_2O} - \mathrm{K_2O})\right] \times 100 \quad (6)$$

Importantly, all three indices are calculated with CaO*, considering only the silicate-bound Ca (Fedo et al., 1995).

CIA, CIW and PIA are all based on the similar assumption that feldspar is the most abundant and reactive mineral, whereas silicate minerals (olivine, pyroxene, amphibole) are proportionally less evident (Nesbitt and Young, 1982). The indices are generally based on the ratio of non-mobile Al to unstable alkali metals and alkaline, thus giving a quantitative measurement of feldspar breakdown. It is important to note, that removal of K from K-feldspar is lower than removal rates of Na and Ca from plagioclase, because plagioclase is more sensitive for weathering than K-feldspar (Nesbitt and Young, 1984; Nesbitt et al., 1996).

However, it is frequently discussed, if K should be used for calculation of WI as it generally shows no consistency during different weathering intensities (e.g. Buggle et al., 2011). This is predominantly caused by the possible absorption of K by clay minerals and the stronger bond by sorptive complexes of soils than for Na or Ca. This may lead to enrichment of K if weathering is weak or vice versa to depletion of K under stronger weathering conditions (Buggle et al., 2011; Harnois, 1988). Accordingly, CIW is the K-free equivalent of CIA, albeit not accounting for the aluminium associated with the K-feldspar. Thus CIW values could be mistakenly high for K-feldspar-rich rocks, whether they are chemically altered or not (Fedo et al., 1995). Respectively, PIA can be used as an index, when only plagioclase weathering needs to be investigated.

CIA data can be displayed in A–CN–K diagrams to display weathering and sorting properties of aluminosilicates (for further explanations see Fig. 3; McLennan, 1993; Nesbitt and Young, 1984; Nesbitt et al., 1996). Numeric values increase with weathering intensity; low values indicate low or absence of chemical alteration as it can be observed under cool or arid conditions (Fedo et al., 1995).

$$\text{Chemical proxy of alteration (CPA)(Buggle et al., 2011; Cullers, 2000)}: \mathrm{CPA}\left(\mathrm{CIW'}\right) = [\mathrm{Al_2O_3}/(\mathrm{Al_2O_3} + \mathrm{Na_2O})] \times 100 \quad (7)$$

CPA (CIW′) tries to avoid all above-discussed biases of carbonate Ca and K-fixation, regarding Na and Al as the most suitable pair of elements to describe weathering intensities (Buggle et al., 2011; Cullers, 2000). Overall, K release is small compared to Na release caused by stronger weathering resistance of K phases such as K-feldspar and clay minerals. This leads to the assumption, that K plays a minor role in the cold climate of the Tibetan Plateau, making this WI a meaningful alternative for our research.

2.5. Pedogenic oxides ratios

Pedogenic oxides are amorphous and crystalline Fe-, Mn-, Al- and Si-oxides, that are formed by chemical weathering and the related genesis of minerals occurring in both soils and sedimentary rocks (Kämpf et al., 2011). For this study, we assessed pedogenic Fe-oxides (PO) by using

several differences and ratios (POR) of the following Fe-fractions to describe the intensity and direction of soil formation processes (Blume and Schwertmann, 1969; Schlichting and Blume, 1962):

- Fet: total iron content (Fe_2O_3)
- Fed: pedogenic (free), well-crystallised iron oxides, hydroxides and oxyhydroxides
- Feo: poorly-crystallised, active and amorphous oxides, hydroxides and oxyhydroxides
- Fep: metalorganic compounds and organically bound Fe (Bascomb, 1968; McKeague, 1967)

The following ratios and differences (POR) were used (for detailed discussion see Section 3.2):

- Fed/Fet: measure for iron release from weathering of primary Fe-bearing minerals (Blume and Schwertmann, 1969; Mirabella and Carnicelli, 1992); the proportion of Fed is higher, the longer and the more intensely weathering processes are persisting
- (Fed-Feo)/Fet: measure for weathering intensities (Alexander, 1985; Arduino et al., 1984); ratio is higher with increasing weathering intensity
- Feo/Fed: degree of activity (Schwertmann, 1964); high ratio indicates high proportion of amorphous oxides, usually showing strong recent weathering of primary silicates in still poorly-developed soils, whereas a low degree of activity refers to dominating well-crystallised iron oxides in comparably more developed soils, both in terms of timeframe and intensity; homogenous substrate for soil formation is an essential precondition for using this ratio
- Fet-Fed: silicate-bound iron in relation to complete iron (Torrent and Cabedo, 1986)
- Fed-Feo: indicates well-crystalised iron oxides (see (Fed-Feo)/Fet)

2.6. Data analyses and statistical applications

All investigated soil profiles (TOTAL), both main and support sites, were allocated to EAST and WEST, respectively. In order to get a better understanding of small-scale pedogenetic processes, one representative main site of each transect was selected for detailed comparison and for establishing continuous catenas. The two sites were chosen in respect of similar geomorphological preconditions, such as relief, hydrology and exposure: Huashixia (E1; HUA) for the eastern transect and Wudaoliang (W1/W2; WUD) for the western transect. TOTAL was bulked into four different soil groups (SG) based on field soil descriptions and laboratory analyses: Regosols (RG), Cambisols (CM), Gleysols (GL), and permafrost-affected soils (PF). It is important to note that the PF soil group does not completely correspond to Cryosols after IUSS Working Group WRB (2006). Properties defined for Cryosols cannot be described for all PF profiles, which is mainly due to the comparably dry environmental conditions. Particularly cryogenic processes leading to cryoturbation, frost heave, temperature cracks or segregation ice are frequently not well-developed outside of lowland areas and valley plains. Hence, profiles where permafrost occurs between 100 and 200 cm, but no cryoturbation features in the first 100 cm (IUSS Working Group WRB, 2006) could be observed were also included in the PF soil group, because similar weathering and soil forming characteristics can be expected in terms of our research approach.

Mean annual air temperature (MAT) and mean annual precipitation (MAP) were calculated based on linear models. Latitude, longitude, and altitude were used as explanatory variables from 50-year averaged temperature and precipitation records (1951–2000) at 680 well-distributed climate stations across China (Fang et al., 2001; He et al., 2006, 2009).

For all sampling groups (TOTAL, EAST, WEST, HUA, WUD, and each SG), the same statistical approaches were conducted. Pearson product moment correlation was performed for WI, PO and their independent variables. The latter include MAT, MAP, SM, ST, pH, $CaCO_3$, TOC, and soil texture classes. On this basis, simple linear regression analyses were performed. Differences between sampling groups were analysed by an independent two-tailed Student's *t*-test. On the basis of an F-test it was decided, whether *t*-test for equal or unequal variances had to be performed. A multiple linear regression approach (MLR) was used to describe the most meaningful linear effects of independent variables on the dependent parameters PO and POR for each sampling group separately. All independent variables were tested for multicollinearity before multiple linear regression analyses were conducted. Thus, we excluded all variables for a single PO/POR with a high interaction ratio ($r > 0.6$; c.f. Table 3—cross-correlation analysis) from the further analysis to avoid interpretations errors. Based on high correlation values, we decided to take only the variable with the most linear relationship to our dependent variable into account. This analysis was done for each sampling group separately.

For diagram construction and statistical analyses SigmaPlot 12 was used. Regression analyses were performed with R software package (R Development Core Team, 2012).

3. Results and discussion

3.1. Weathering indices (WI)

3.1.1. Synopsis of weathering indices

Calculated WI are shown in multi-panel Fig. 2, together with the most significant POR as well as $CaCO_3$ and NaCl contents. Essentially, three groups of WI can be separated: PI and KN; CIA, CIW and PIA; as

Table 2
Descriptive statistics of selected parameters (SM, CaCO3 and TOC all %; Feo, Fed and Fet all ‰); ordered by parameters for comparison between sampling groups. See S2 in the electronic supplementary data for the detailed version.

Group	Parameter	n	Range	Mean	Std. Dev.	Min	Med.	Max
EAST	SM	38	70.20	43.29	15.85	6.20	47.30	76.40
WEST	SM	57	67.50	31.43	16.46	4.00	32.50	71.50
HUA	SM	21	70.20	49.94	14.69	6.20	50.00	76.40
WUD	SM	18	21.30	43.21	6.70	32.00	44.15	53.30
RG	SM	10	29.80	16.63	8.49	6.20	15.05	36.00
CM	SM	20	29.60	18.26	9.90	4.00	16.40	33.60
GL	SM	29	48.40	44.04	11.64	10.40	48.00	58.80
PF	SM	36	59.20	45.21	13.51	17.20	42.85	76.40
EAST	$CaCO_3$	52	17.96	8.95	5.78	0.00	8.31	17.96
WEST	$CaCO_3$	74	24.73	10.96	6.43	0.19	13.37	24.92
HUA	$CaCO_3$	28	11.74	5.76	3.29	0.45	6.36	12.19
WUD	$CaCO_3$	28	3.63	14.64	0.81	13.36	14.70	16.99
RG	$CaCO_3$	10	20.21	15.48	6.68	4.71	16.50	24.92
CM	$CaCO_3$	26	17.26	9.54	6.26	0.19	13.13	17.45
GL	$CaCO_3$	38	17.56	10.50	4.81	0.40	10.57	17.96
PF	$CaCO_3$	52	22.95	9.12	6.65	0.00	10.42	22.95
HUA	TOC	28	18.13	3.32	3.94	0.15	2.29	18.28
WUD	TOC	28	5.83	1.26	1.26	0.41	0.85	6.24
RG	TOC	10	3.16	0.74	0.93	0.00	0.36	3.16
CM	TOC	26	7.15	1.44	1.69	0.24	0.75	7.39
GL	TOC	38	12.43	2.32	2.47	0.19	1.55	12.62
PF	TOC	52	18.23	3.23	4.19	0.05	1.20	18.28
HUA	Fe o	27	5.60	3.30	1.70	1.18	2.93	6.78
WUD	Fe o	28	1.66	1.33	0.40	0.71	1.29	2.37
RG	Fe o	10	2.13	0.98	0.74	0.19	0.65	2.33
CM	Fe o	26	2.95	1.13	0.72	0.46	0.81	3.40
GL	Fe o	37	7.35	3.58	2.02	0.79	3.37	8.14
PF	Fe o	52	6.57	1.94	1.25	0.22	1.44	6.78
HUA	Fe d	27	12.17	5.82	2.89	2.44	5.17	14.61
WUD	Fe d	28	4.79	7.36	1.15	5.90	6.94	10.69
RG	Fe d	10	7.43	6.43	2.28	3.75	5.69	11.18
CM	Fe d	26	11.06	8.68	2.90	3.30	8.30	14.36
GL	Fe d	37	14.25	6.40	3.63	1.39	6.65	15.64
PF	Fe d	52	15.31	7.62	2.92	3.56	6.85	18.87
HUA	Fe t	27	34.93	44.26	7.52	25.88	43.33	60.81
WUD	Fe t	28	11.79	33.55	3.21	27.78	33.16	39.57
RG	Fe t	10	34.49	33.01	10.21	19.58	29.45	54.07
CM	Fe t	26	31.72	39.88	11.52	23.92	33.83	55.64
GL	Fe t	37	31.72	41.50	7.43	25.82	40.62	57.54
PF	Fe t	52	40.13	36.73	8.20	20.68	34.58	60.81

Table 3
Product–moment correlation coefficients (Pearson) for the most important site variables. The significance is marked (**p < 0.01; *p < 0.05; others p > 0.05).

	MAP [mm a^{-1}]	SM [vol. %]	ST [°C]	pH [$CaCl_2$]	$CaCO_3$ [%]	TOC [%]	Sand [%]	Silt [%]	Clay [%]	Fe t [‰]	Fe d [‰]	Fe o [‰]	Fe p [‰]
MAT [°C]	0.33**	−0.41**	0.48**	−0.04	−0.19*	0.03	−0.04	−0.22*	0.47**	0.48**	0.33**	0.19*	0.03
MAP [mm a^{-1}]		0.07	0.15	−0.39**	−0.63**	0.32**	0.08	−0.15	0.11	0.25**	−0.16	0.40**	0.37**
SM [vol. %]			−0.39**	−0.16	−0.13	0.39**	−0.49**	0.62**	−0.05	−0.12	−0.33**	0.48**	0.50**
ST [°C]				0.02	−0.13	0.10	0.09	−0.21	0.18	0.04	0.10	−0.11	−0.01
pH [$CaCl_2$]					0.71**	−0.54	0.16	−0.02	−0.29**	−0.02	−0.28**	−0.22*	−0.55**
$CaCO_3$ [%]						−0.53**	0.08	0.06	−0.27**	−0.25**	−0.25**	−0.38**	−0.53**
TOC [%]							−0.23*	0.12	0.27**	−0.22*	−0.02	0.38**	0.89**
Sand [%]								−0.88**	−0.52**	−0.49**	−0.22*	−0.33**	−0.27**
Silt [%]									0.04	0.22*	0.02	0.28**	0.20*
Clay [%]										0.62**	0.43**	0.19*	0.21*
Fe t [‰]											0.47**	0.28**	−0.16
Fe d [‰]												0.02	−0.02
Fe o [‰]													0.55**

	PI	KN B	CIA	CIW	PIA	FENG	CPA	Fed/Fet	Feo/Fed	(Fed-Feo)/Fet
MAT [°C]	−0.30**	−0.35**	0.47**	0.41**	0.46**	0.73**	0.51**	−0.01	0.02	−0.04
MAP [mm a^{-1}]	−0.39**	−0.61**	0.42**	0.37**	0.42**	0.39**	−0.02	−0.33**	0.41**	−0.45**
SM [vol.%]	−0.04	0.00	−0.06	−0.06	−0.07	−0.34**	−0.14	−0.29**	0.47**	−0.50**
ST [°C]	−0.17	−0.12	0.06	0.02	0.06	0.22	−0.02	0.04	−0.18	0.09
pH [$CaCl_2$]	0.78**	0.67**	−0.5**	−0.52**	−0.51**	−0.42**	−0.33**	−0.35**	0.01	−0.15
$CaCO_3$ [%]	0.85**	0.93**	−0.71**	−0.71**	−0.72**	−0.50**	−0.24**	−0.14	−0.12	0.06
TOC [%]	−0.60**	−0.37**	0.10	0.08	0.10	0.08	0.10	0.15	0.20*	−0.16
Sand [%]	0.07	0.18	−0.34**	−0.32**	−0.31**	−0.13	−0.51**	0.08	−0.21*	0.2*
Silt [%]	0.09	0.04	0.07	0.05	0.04	−0.15	0.14	−0.16	0.29**	−0.26**
Clay [%]	−0.31**	−0.44**	0.57**	0.56**	0.57**	0.54**	0.80**	0.11	−0.08	0.04
Fe t [‰]	−0.14	−0.49**	0.74**	0.71**	0.73**	0.62**	0.68**	−0.13	0.06	−0.11
Fe d [‰]	−0.41**	−0.42**	0.53**	0.54**	0.53**	0.58**	0.60**	0.79**	−0.52**	0.71**
Fe o [‰]	−0.28**	−0.34**	0.26**	0.24**	0.25**	0.13	0.13	−0.18	0.72**	−0.59**
Fe p [‰]	−0.54**	−0.39**	0.15	0.13	0.14	0.07	0.07	0.10	0.34**	−0.26**
PI		0.81**	−0.66**	−0.66**	−0.66**	−0.65**	−0.44**	−0.40**	0.04	−0.17
KN B			−0.89**	−0.88**	−0.89**	−0.70**	−0.46**	−0.17	−0.06	−0.01
CIA				0.99**	1.00**	0.82**	0.70**	0.12	0.01	0.05
CIW					1.00**	0.77**	0.70**	0.15	−0.02	0.09
PIA						0.81**	0.70**	0.13	0.00	0.06
FENG							0.76**	0.24**	−0.14	0.20*
CPA								0.26**	−0.16	0.21*
Fed/Fet									−0.63**	0.88**
Feo/Fed										−0.87**

well as CPA and FENG. Curves for PI and KN B show close dependency to $CaCO_3$ contents, since Ca was not corrected for these indices, which makes their interpretation difficult (cf. Section 2.4). At sites, where carbonate contents do not vary much (cf. site W1), PI and KN B are basically comparable to the other indices.

For all investigated sites, CIA, CIW and PIA plot largely parallel with no differences in indicating the tendency of weathering or changes of substrate layers within soil profiles. Accordingly, consideration of K does not make any difference for the investigated region, which is mainly due to the stronger weathering resistance of K phases, particularly in periglacial regions with overall low weathering intensities (Buggle et al., 2011; Cullers, 2000). Similarly, feldspars are mainly represented by plagioclases as can be proved by the A-CN-K diagrams (Fig. 3, Fedo et al., 1995). Because CaO* was used for these indices, curves are not directly linked to $CaCO_3$ contents, thus offering more reliable results than PI and KN for the investigated substrates. Hereafter, CIA is mentioned representatively for all CIA, CIW and PIA.

Ca-free indices CPA and FENG show better differentiation for some sites where other indices plot relatively homogenous (e.g. W2). Nevertheless, the depth function of CPA for other profiles is overall smoother and does not show extreme peaks, such as in E1 A, E1 D or E1 E. Since increased salinity occurs especially in topsoils of sites with negative water balance (Scheffer et al., 2002), a misinterpretation of CPA may happen with the result of an overall underestimated weathering intensity due to higher Na contents (Buggle et al., 2011). The higher sensitivity to recent climate conditions and corresponding salinity is related to the exclusive use of Al and Na for calculation of CPA, thus giving Na a higher relative importance.

Changes of substrate layers in soil profiles indicated by amplitudes of WI were compared to soil physical and chemical analyses (grain size distribution and skeleton content, carbonate content, TOC). Accordingly, reasonable and verified layer changes are marked in Fig. 2 (LC). WI generally indicate weathering trends with soil depth, but also layering (e.g. E1). However, CPA depicts some problems with salinity in several topsoil horizons (e.g. W2 A1, W3 A1, W6 B1, and W6 G1). The most pronounced and partly contradictory results of CIA and Ca-free indices can be observed in the area around Nagqu (W6): here, well-developed soils on sporadic permafrost and seasonally frozen ground are influenced by a stronger Tropical Monsoon. Site W6 A is highlighting this issue very clearly with opposite weathering trends indicated by both WI groups. Importantly, NaCl enrichment is not very pronounced at this site, but confirming the trend of CPA. The CIA decreases with depth, indicating a lower weathering intensity; this is supported by a simultaneously increasing $CaCO_3$ content with soil depth. Beside carbonatic parent material, this increase is caused by translocation of $CaCO_3$ to deeper soil layers associated with higher rainfall and warmer temperatures in the Nagqu region (Table 1). Illuviated $CaCO_3$ can be observed in the form of carbonate pseudo-mycelia and even small concretions. Nevertheless, this evidence for pedogenesis does not equal to higher weathering rates in terms of silicate mineral weathering processes. Higher carbonate contents lead to higher pH values above the silicate buffer, hence preventing extensive silicate weathering processes. The POR (Fed-Feo)/Fet suggests the same tendency as CIA. Similar observations can be discussed exemplary for the change of layer in horizon W6 C3 and for profile W6 E, although salinity has also no influence at these sites.

These results show, that CIA is a most reliable index, if laboratory data of $CaCO_3$ contents are available for the calculation of CaO*.

Frequently, lower weathering intensities in the surface horizons are evident. One explanation is the high organic content and felty structure built up by fine roots in topsoils of *Kobresia* meadows (Kaiser et al., 2008). These turf-like horizons comprise proportionally less in-situ weathered mineral soil material, often disconnected from the organo-mineral soil body, additionally acting easily as a trap for fresh airborne sediments. In most cases, comparably fresh aeolian sediment input on top of the soil surface is evident. The aeolian sediment is mainly derived from rather proximal source areas affected by strong permafrost degradation processes leading to layering (Baumann et al., 2009; Yang et al., 2010). One has to be aware, that sorting effects of different substrates can also account for shifts of weathering indices, even though no differences of weathering intensities are evident (Nesbitt et al., 1996). Nevertheless, variation of substrate composition mostly shows no extremes in the research area, neither in agents, nor in texture. Profile E1 A provides a good example of the above mentioned possibilities of changes in depth functions due to substrate layering: weathering intensity increases from horizon E1 A2 to E1 A3. This is mainly caused by layering, with higher aeolian derived silt content in the topsoil. Abrupt transitions to lower weathering intensities can also be explained by layering: the substrate of horizon E1 A4 consists of fluvial deposits with a high content of rock fragments (>2 mm). In profiles E1 D and E1 E these characteristics are also evident, with higher silt contents and organic matter contents in the topsoils.

POR are easily influenced by strong short-term redox processes overprinting rather long-term weathering processes (Fiedler and Sommer, 2004). Thus, the depth function for (Fed-Feo)/Fet does not apply well to soil horizons influenced by redox processes. Accordingly, Price and Velbel (2003) comment the use of Fe for WI critically due to the change in solubility when Fe^{3+} changes valence to Fe^{2+} (cf. FENG). Accordingly, Al-based WI can be regarded as more appropriate. The depth functions of profile W1 A can be best explained by a mixed influence of redox processes and permanently frozen horizons, because layering could not be identified.

Site W2 is crucial for the discussion of different characteristics of WI. The depth function of CPA is very similar to that of $CaCO_3$ and well corresponding to POR, whereas other indices show much smaller magnitudes and do not indicate all layer changes. However, the high salinity of horizon W2 A1 originated from capillary evaporation to the surface lowers the CPA. Generally, this supports the idea that related to environmental conditions; it should be a site-specific decision, which WI is most appropriate. All in all, the CIA plots the most comprehensible results.

Specific climatic trends and site conditions are traced very clearly by the plots (higher MAT and MAP from N to S and W to E) when comparing EAST and WEST. While the oscillation of the depth functions is generally high in the zone of discontinuous permafrost of EAST, sites located in regions with continuous permafrost conditions (W1 and W2) show only very small changes in weathering intensities due to stable temperature–moisture (Zhang et al., 2003) as well as sedimentary

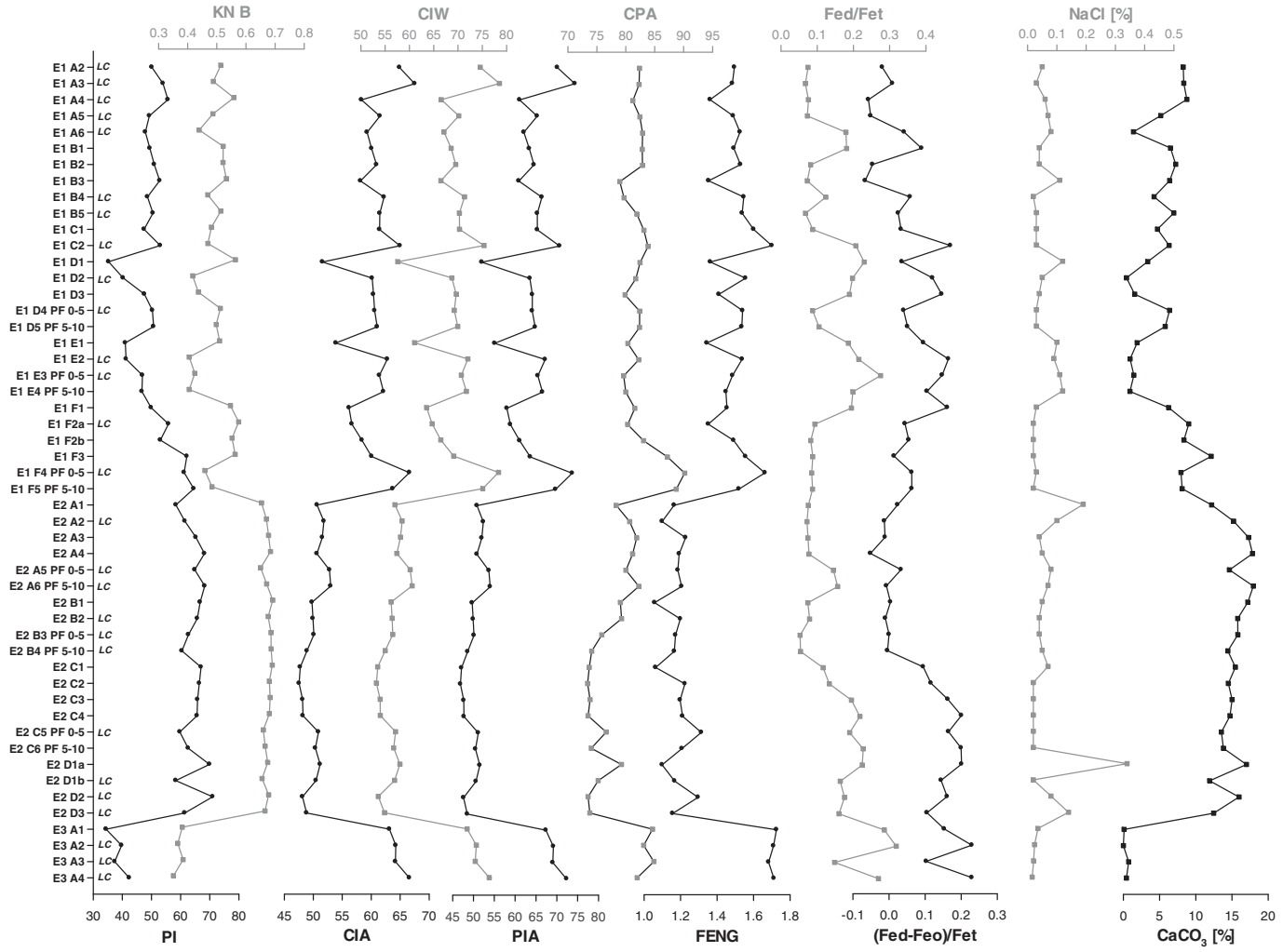

Fig. 2. Parallel plots of WI for transect EAST (Fig. 2a) and WEST (Fig. 2b). WI grouped according to similar characteristics: PI/KN B, CIA/CIW/PIA, CPA/FENG. The most significant POR together with NaCl and $CaCO_3$ contents are plotted. Changes of layers are indicated by "*LC*". Sites are ordered for each transect from N to S.

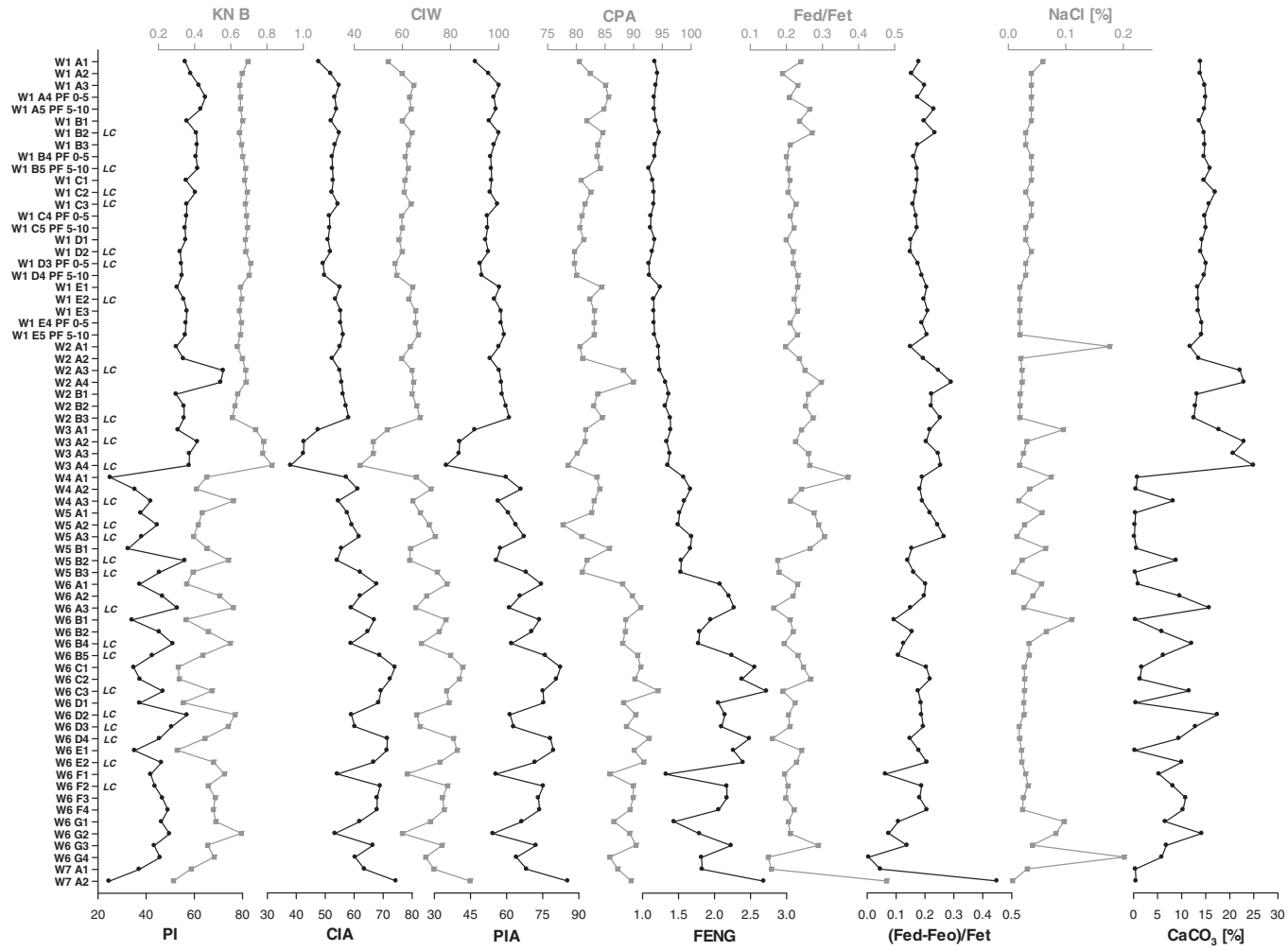

Fig. 2 (*continued*).

conditions (Baumann et al., 2009). The influence of the Tropical Monsoon is increasing further south on the western transect (sporadic permafrost mixed with seasonally frozen ground at W6–W7), with higher MAT and MAP (Domrös and Peng, 1988). This climate trend leads again to higher oscillations of the depth function of WI along WEST in southern direction. Data of EAST also gives an impression of different weathering dynamics at sites where permafrost has been degraded (E2) with clearly more homogenous conditions and lower weathering intensity caused by different soil moisture interrelations (Baumann et al., 2009; Xue et al., 2009).

3.1.2. A–CN–K ternary plots and chemical index of alteration (CIA)

CIA is the most reliable WI with the highest explanatory power. The elements used for calculation of the CIA can be plotted in A–CN–K ternary diagrams, visualising scattering in-between sampling groups (Nesbitt et al., 1996). This gives information with regard to weathering intensity and homogeneity of parent material (Fig. 3; Buggle et al., 2011). It also provides a basis to decide, if results of the sampling groups can be compared and interpreted together as well as brought into the context for a common discussion. Supplementary to the diagrams, descriptive statistics for the A–K, CN–K and A–CN joins were calculated to gain average values of weathering intensities and a measure of dispersion for the indicators (Table 4; McLennan, 1993). Generally speaking, the A–K join is a measure for weathering intensity and can be equalled with CIA values, whereas the CN–K join displays the parent material and its homogeneity (shift along the feldspar join). The degree of parallelism to the A–CN join indicates to what extend other minerals than plagioclases are the source of the weathering lines (Nesbitt and Young, 1984; Nesbitt et al., 1996).

TOTAL exhibits a wide range of weathering intensities (Fig. 3a). Interestingly, almost 25% of the samples plot below or only slightly above the feldspar join, indicating essentially no weathering. Moreover, other minerals, such as amphiboles or pyroxenes derived from mafic–ultramafic rocks are relevant in the unweathered material besides feldspars (Nesbitt and Young, 1984). Half of the samples are not or only slightly weathered, whereas the second quartile and the maximum value highlight sites with comparably intense weathering conditions. The median of the CN–K join shows a small shift from the UCC (upper continental crust) average towards K-feldspar, but with plagioclase being predominant (Table 4).

The two main investigation sites are compared in Fig. 3b. HUA (E1) reflects with clearly higher range and variance of weathering intensities the more diverse conditions in discontinuous permafrost environments. It shows a distinct feldspar weathering line with no results below the feldspar join. As indicated by the higher median, there is—compared to TOTAL—an enhanced weathering intensity evident. WUD (W1 and W2) reveals overall very low weathering intensities, being on average clearly below TOTAL with a maximum showing no distinct weathering signs (Nesbitt and Young, 1982). The range and variance is much smaller than in HUA underlining the above-mentioned lower weathering intensity and higher homogeneity of site characteristics in continuous permafrost landscapes. The CN–K join indicates very homogenous parent material with low scattering (cf. standard deviation and variance) and the mean reveals a shift towards K-feldspar compared to HUA.

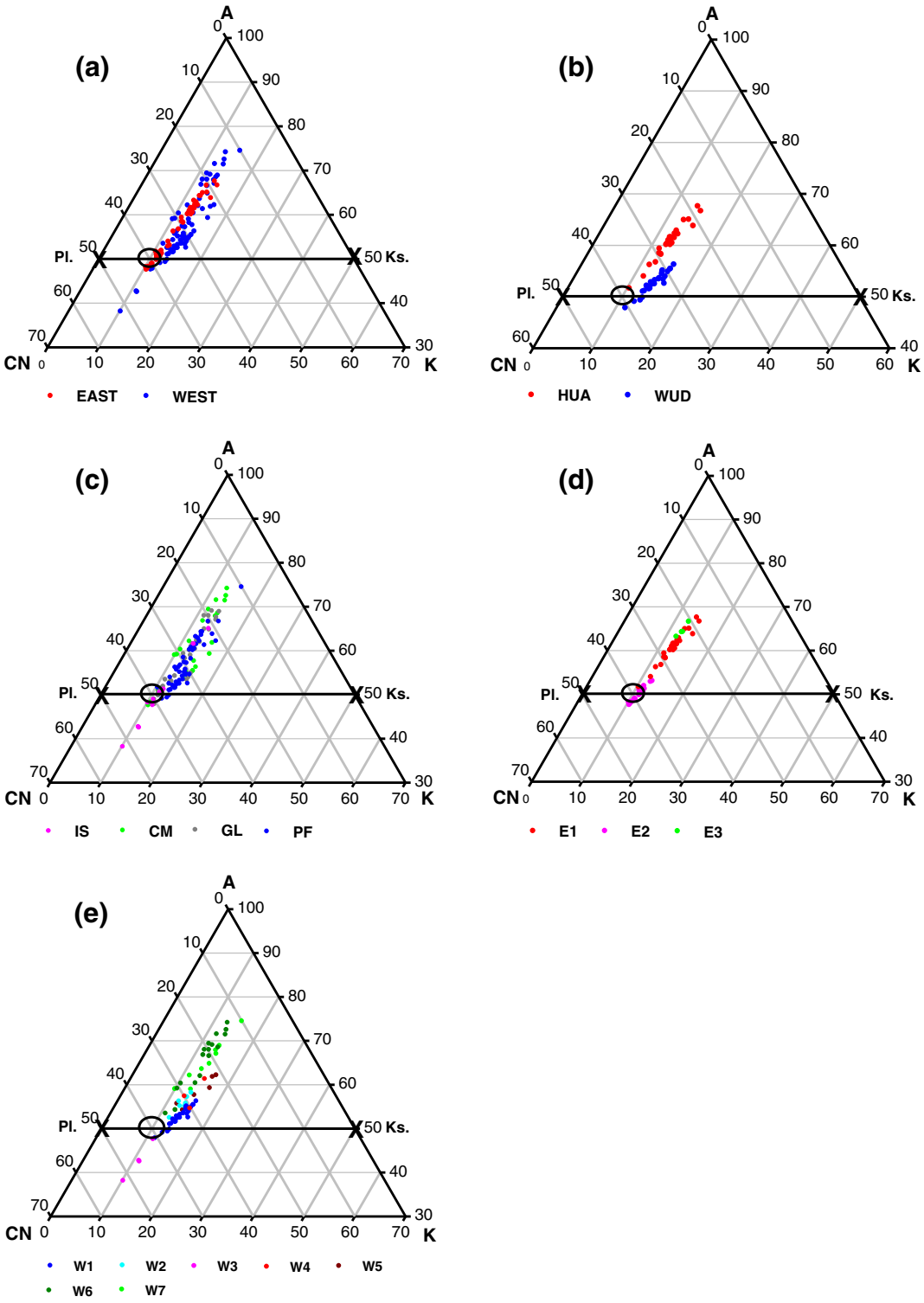

Fig. 3. A–CN–K [Al_2O_3–(CaO^* + Na_2O)–K_2O] ternary diagrams according to Nesbitt and Young (1984). Only the sections within the value range are displayed. Diagrams are plotted for the following sampling groups: a) TOTAL and EAST/WEST; b) Main comparison sites: HUA (E1)/WUD (W1/2); c) Soil groups: IS, CM, GL, PF; d) Main study sites EAST: E1, E2, E3; e) Main study sites WEST: W1/W2, W3, W4, W5, W6/W7. The feldspar join between plagioclase (Pl.) and K-feldspar (Ks.) as well as the average position of the upper continental crust (McLennan, 2001) are indicated in the diagrams.

The two main sites thus can be explicitly differentiated in terms of parent material. The parallelism to the A–CN join differs between HUA and WUD. While HUA is only slightly oblique towards the A–K join, WUD differs much stronger in the same direction indicating that also other minerals than plagioclase are involved in the weathering processes particularly at WUD.

Scattering along the CN–K join of the two main sites and TOTAL indicates homogenous conditions of parent materials within the sites HUA and WUD. Compared to their standard deviation and variance, scattering of TOTAL can still be considered as moderate. Thus the results of TOTAL can be well discussed and interpreted to observe general trends.

Table 4
Descriptive statistics for A–K, CN–K and A–CN joins of ternary diagrams (cf. Fig. 3).

Sample	Join	n	Range	Mean	Var.	Std. Dev.	Min	1. Q	Med.	3. Q	Max
TOTAL	A–K	125	36.33	57.22	50.22	7.09	38.08	51.84	56.17	61.91	74.42
	CN–K	125	6.77	12.93	2.20	1.48	10.07	11.73	12.89	13.86	16.84
	A–CN	125	41.58	29.85	58.71	7.66	10.04	24.50	30.46	34.97	51.62
EAST	A–K	51	19.98	56.77	38.51	6.21	47.54	50.65	58.32	61.50	67.52
	CN–K	51	4.94	12.17	1.14	1.07	10.22	11.40	12.35	12.76	15.16
	A–CN	51	23.41	31.06	51.14	7.15	18.42	25.70	29.31	38.15	41.83
WEST	A–K	74	36.33	57.53	58.69	7.66	38.08	52.50	55.35	62.04	74.42
	CN–K	74	6.77	13.45	2.28	1.51	10.07	12.43	13.57	14.31	16.84
	A–CN	74	41.58	29.02	62.97	7.94	10.04	23.52	30.55	33.68	51.62
HUA	A–K	0	15.93	60.61	12.45	3.53	51.59	58.84	60.92	62.17	67.52
	CN–K	0	4.71	12.75	0.95	0.98	10.45	12.38	12.53	13.13	15.16
	A–CN	0	19.54	26.64	19.14	4.37	18.42	24.72	26.34	29.17	37.96
WUD	A–K	28	8.45	52.59	4.27	2.07	47.76	51.53	52.50	54.02	56.21
	CN–K	28	4.19	14.14	1.02	1.01	11.71	13.50	13.97	14.73	15.90
	A–CN	28	12.40	33.27	8.73	2.96	28.13	30.98	33.41	34.78	40.53
IS	A–K	10	26.89	49.58	68.74	8.29	38.08	43.87	48.49	51.00	64.97
	CN–K	10	3.58	11.51	1.13	1.06	10.22	11.03	11.36	11.74	13.79
	A–CN	10	30.39	38.91	85.19	9.23	21.23	37.27	40.57	45.08	51.62
CM	A–K	26	26.55	59.58	70.87	8.42	47.54	53.93	59.01	67.53	74.09
	CN–K	26	6.77	12.84	4.31	2.08	10.07	10.81	12.48	14.47	16.84
	A–CN	26	28.80	27.58	82.37	9.08	13.02	19.68	28.63	31.68	41.83
GL	A–K	37	21.25	58.00	44.25	6.65	47.76	51.91	58.32	62.21	69.01
	CN–K	37	4.33	12.66	1.43	1.20	11.02	11.68	12.44	13.31	15.35
	A–CN	37	23.29	29.35	51.28	7.16	17.24	24.50	29.30	35.58	40.53
PF	A–K	52	25.40	56.96	29.20	5.40	49.02	52.48	55.66	61.10	74.42
	CN–K	52	6.19	13.44	1.32	1.15	10.45	12.72	13.33	13.99	16.64
	A–CN	52	28.35	29.60	32.16	5.67	10.04	26.04	30.96	33.74	38.38

The comparison of EAST and WEST is plotted in Fig. 3a. WEST displays a broader range of weathering intensities than EAST, because the western transect crosses more climatic regions, including sites of discontinuous, continuous and south of Tanggula Shan even sporadic permafrost with well-developed Cambisols. Comparable sites with intense soil formation are missing in EAST. On the other hand, EAST comprises no sites influenced by continuous permafrost without detectable current weathering processes, such as in WUD. This approximates the average weathering intensities (cf. mean and median) of EAST and WEST, but leads to a much greater variance for WEST. Moreover, the two transects are also clearly different in terms of parent material with a much higher variation in WEST. To summarise, WEST displays equal scattering to TOTAL, which underlines the greater variety of soil forming processes for WEST.

Concerning SG (Fig. 3c), homogeneity (CN–K join) cannot be interpreted, because regional variations of parent materials are determining this parameter and SG are spread throughout many sites of the investigation area. Additionally, regional clustering of particular SG is biasing the values.

Environments with soils strongly affected by permafrost have generally low weathering potentials with rather homogenous conditions compared to other regions (Kimble, 2004). Under moist and cold conditions chemical weathering processes are slowed down (Brady and Weil, 2008; McLennan, 1993). Accordingly, the lowest dispersion of weathering intensities can be referred to PF (Fig. 3c). RG and CM exhibit clearly differing weathering intensities with CM having the highest and RG the lowest values of all soil groups. GL and PF indicate slightly lower weathering than CM.

Climatic trends and permafrost condition along both transects can be highlighted by the data plotted in Fig. 3d and e. Transect EAST (Fig. 3d) shows an increasing weathering trend from E2, E1, to E3, which is coincident to the climatic gradient (increasing MAT and MAP). Moreover, especially because E2 and E1 are located close to each other, vegetative cover and permafrost characteristics become even more important: E2 reveals turbulent environmental conditions with alternate erosion and deposition that result in sparse vegetation, which in turn favours again erosional processes. This feedback is triggered by a comparably thick active layer, implicating corresponding drier conditions. The frequently occurring translocation processes lead to syngenetic weathering and soil formation (Dietze et al., 2012), resulting in very low in-situ weathering values.

Transect WEST encompasses a wide variation of climate conditions and parent materials over a long distance (cf. CN–K join for W1/W2 and W6/W7). Sites can be likewise ordered by their geographical location with the exception of W3, which features only one profile with initial soil formation as soil conditions did not change for several kilometres in this area. All horizons plot below the feldspar join, indicating minimal weathering. The other sites show a clear differentiation: WUD (W1/W2) is situated in an area with continuous permafrost and low precipitation, W4 is located south of Tanggula Pass in the transition zone from continuous to discontinuous permafrost with rising MAP and influenced by the Tropic Monsoon, and W5 is finally situated in discontinuous permafrost. W6/W7 are already strongly influenced by the Tropic Monsoon with prevailing sporadic permafrost conditions and seasonally frozen ground.

3.1.3. Statistical differences between sampling groups

Table 5 lists significantly different sampling groups as a result of two-tailed t-tests with $p < 0.05$ for each WI. For CIA, CIW, PIA and KN B, overall the same groups can be considered as significantly different. The only, but very crucial discrepancy of these indices to CPA is that for CPA, EAST and WEST are calculated as significantly different but not HUA and WUD. However, the distinct differences in weathering intensities of HUA and WUD were shown very clearly by the ternary diagrams (Fig. 3b). According to CIA, differences along each transect are more distinct than differences between EAST and WEST, which can be supported by the ternary diagrams. This also shows that CPA is not the appropriate WI for the investigated sites. SG can be distinguished only including RG as the soil group with the lowest weathering intensities. It is important to note that KN Index B shows—although not calculated with CaO^*—exactly the same differences than CIA. This underlines the principally similar characteristics of KN Index B and CIA as a measure of feldspar breakdown (cf. Fig. 2; Buggle et al., 2011; Kronberg and Nesbitt, 1981).

Table 5
Student's *t*-test for most important WI, PO, and POR between sampling groups (only sig. tests shown). The level of significance is marked (***p < 0.001; **p < 0.01; *p < 0.05).

Parameter	Group 1	Group 2	F-test/variance	t-statistic	t-critical
CIA	HUA	WUD	Unequal	10.233	2.018***
CIA	RG	CM	Unequal	−3.226	2.110**
CIA	RG	PF	Unequal	−2.705	2.201*
CIA	RG	GL	Equal	−3.368	2.014**
CIW	HUA	WUD	Unequal	7.692	2.015***
CIW	RG	CM	Equal	−3.295	2.032**
CIW	RG	PF	Unequal	−2.935	2.228*
CIW	RG	GL	Equal	−3.438	2.014**
PIA	HUA	WUD	Unequal	9.549	2.018***
PIA	RG	CM	Unequal	−3.233	2.110**
PIA	RG	PF	Unequal	−2.713	2.201*
PIA	RG	GL	Equal	−3.305	2.014**
CPA (CIW′)	East	West	Unequal	−6.249	1.982***
CPA (CIW′)	RG	CM	Unequal	−2.850	2.042**
CPA (CIW′)	RG	PF	Unequal	−3.122	2.201**
CPA (CIW′)	RG	GL	Unequal	−3.269	2.120**
KN B	HUA	WUD	Unequal	−10.233	2.018***
KN B	RG	CM	Unequal	3.226	2.110**
KN B	RG	PF	Unequal	2.705	2.201*
KN B	RG	GL	Equal	3.368	2.014**
(Fed-Feo)/Fet	East	West	Unequal	−8.189	1.989***
(Fed-Feo)/Fet	Hua	Wud	Unequal	−8.784	2.037***
(Fed-Feo)/Fet	GL	PF	Unequal	−5.325	1.995***
(Fed-Feo)/Fet	CM	PF	Unequal	2.606	1.992*
(Fed-Feo)/Fet	RG	GL	Unequal	4.303	2.101***
(Fed-Feo)/Fet	CM	GL	Unequal	7.912	2.008***
Fed/Fet	East	West	Unequal	−7.710	1.990***
Fed/Fet	Hua	Wud	Unequal	−6.675	2.040***
Fed/Fet	GL	PF	Unequal	−4.104	1.991***
Fed/Fet	RG	GL	Unequal	2.475	2.101*
Fed/Fet	CM	GL	Unequal	4.731	2.000***
Fep	Hua	Wud	Unequal	3.833	2.045***
Fep	CM	PF	Unequal	−3.942	2.000***
Fep	RG	PF	Unequal	−4.328	2.000***
Fep	RG	GL	Unequal	−4.858	2.014***
Fep	CM	GL	Unequal	−4.467	2.013***

3.1.4. Correlations and simple regressions between WI and control variables

No significant correlations are evident between WI and SM, albeit MAP and MAT display good relationships (Table 3). One explanation is that long-term average data are more related to WI than short-term alternating parameters, such as SM or TOC. Moreover, since MAT and MAP do not vary within main sites compared to the other independent variables, site-specific differences related to parent material and other particular environmental conditions are indirectly traced by these findings (cf. Fig. 3). Other common features of CIA, PIA CIW, CPA and FENG are the pronounced negative relationship to soil acidity parameters, i.e. higher weathering intensities with lower pH and $CaCO_3$ contents, and the positive correlation to clay (for PI and KN vice versa). Accordingly, increased weathering intensity can be related to higher acidity and clay content as a product of feldspar breakdown (Nesbitt and Young, 1984). No significant correlations to silt are observable, but sand is negatively correlated to CIA, PIA CIW and CPA. Sandy material is excessively drained and very low in water holding capacity.

The above described corresponding depth function of different WI (Fig. 2) can be confirmed by correlation analyses among them. Essentially, CIA, PIA and CIW plot almost identical ($r = 0.99$) for the investigated sites. Their relationships with the carbonate-free CPA and FENG are weaker (e.g. $r = 0.70$ for CPA). Interestingly, even if CaO is not corrected for KN B, the correlation of CIA and KN B is high, whereas PI only indicates a medium relationship. These findings are related to the different principles of these indices (Duzgoren-Aydin et al., 2002 and Section 2.4). The strong correlation of KN B with $CaCO_3$ however, leads to the conclusion, that WI using Ca without correction are biased to a large extent by calcium carbonate contents and therefore can be not considered as useful for TOTAL, EAST and WEST sampling sets, which have no or rather different calcium carbonate contents.

Based on the correlation analyses with independent variables, clay and $CaCO_3$ contents were selected for simple regression analyses to explain the variation of CIA within each sampling group (Table 6). For TOTAL, 32% of CIA variation can be positively explained by clay content. Comparing the two transects, WEST has a higher R^2, mainly because this transect includes more sites with well-developed Cambisols (CM) and higher weathering intensities (W6/W7). Altogether, CM expresses the highest R^2 with 65% of explained variance, referring to the soil group with the highest degree of weathering. Hydrolysis of silicates and formation of clay minerals, being major soil formation processes of Cambisols (Brady and Weil, 2008; Jenny, 1994), are responsible for clay enrichment and the strong relationship between CIA and clay content for CM (Nesbitt et al., 1996). However, type and abundance of clay minerals can bias the chemical elements ratios along the weathering profile, particularly when they originate from clay-rich parent material (Duzgoren-Aydin et al., 2002; Nesbitt and Young, 1984). Indeed, clay contents of parent material are generally low in the investigated area on the Tibetan Plateau, with soil mostly developed in a surface layer dominated by fine sands and silts which may relativise the error. GL only exhibits 16% of explained variance, as weathering in GL is inhibited for a certain period at ground water influenced sites and weathering products are redistributed frequently within profiles (Fiedler and Sommer, 2004). Furthermore, constant lateral supply with fresh or diversely pre-weathered compounds is likely, as GL soils are commonly located in geomorphological depressions or valleys (Brady and Weil, 2008). To a less extend, similar arguments can be taken for permafrost-affected soils (PF). No significant relationships are evident for RG because of predominantly fresh aeolian sediments with very low primary and secondary clay contents (Baumann et al., 2009; Yan et al., 2009).

The strong affinity of CIA and $CaCO_3$ content was clearly described in Fig. 2. $CaCO_3$ as an indicator for soil alkalinity is one of the major parameters for soil weathering processes: the higher the $CaCO_3$ content, the lower the weathering intensity. Accordingly, the different sampling groups show high negative explained variances with higher acidity leading to enhanced weathering intensities. The highest value of 89% explained variance can be observed for RG, which is essentially due to the overall comparably high carbonate contents and insignificant clay contents (cf. Table 2 and electronic supplementary data S2, descriptive statistics) combined with very low weathering processes at these sites. Remarkably, carbonate dynamics within WUD and HUA are not high enough to show significant relationships.

Table 6
Simple regression analyses for CIA. The level of significance is marked (*** p < 0.001; ** p < 0.01; * p < 0.05; others p > 0.05). Direction of change is indicated by (+) for positive and (−) for negative influence.

Group	Parameter x	Parameter y	n	R^2	Std. Error Regression
TOTAL	CIA	Clay	112	0.32*** (+)	7.67
EAST	CIA	Clay	45	0.24*** (+)	8.65
WEST	CIA	Clay	66	0.40*** (+)	6.48
HUA	CIA	Clay	21	0.04 (+)	11.76
WUD	CIA	Clay	20	0.34** (+)	3.69
RG	CIA	Clay	8	0.00 (−)	6.30
CM	CIA	Clay	24	0.65*** (+)	5.83
GL	CIA	Clay	35	0.16* (+)	8.33
PF	CIA	Clay	42	0.27*** (+)	7.82
TOTAL	CIA	CaCO3	124	0.51*** (−)	4.40
EAST	CIA	CaCO3	50	0.60*** (−)	3.74
WEST	CIA	CaCO3	73	0.51*** (−)	4.54
HUA	CIA	CaCO3	26	0.03 (+)	3.11
WUD	CIA	CaCO3	27	0.03 (−)	0.81
RG	CIA	CaCO3	9	0.89*** (−)	2.36
CM	CIA	CaCO3	25	0.44*** (−)	4.76
GL	CIA	CaCO3	36	0.53*** (−)	3.38
PF	CIA	CaCO3	51	0.50*** (−)	4.77

3.2. Pedogenic oxides (PO) and pedogenic oxides ratios (POR)

3.2.1. Correlations between PO, POR, control variables, and WI

(Fed-Feo)/Fet shows the highest negative correlations with moisture parameters (Table 3), whereas no significant relationships are displayed for soil acidity. In contrast, Fed/Fet exhibit lower correlation coefficients for MAP and SM, but a high negative correlation with pH. Overall, the degree of activity (Feo/Fed) (Schwertmann, 1964), reacts contrarily with positive relations to moisture conditions (for a general discussion see Section 3.2.3).

Fep has the highest and most significant correlation with TOC contents ($r = 0.89$). This clearly supports the idea, that pyrophosphate extracts mainly organically bound iron (Bascomb, 1968; McKeague, 1967). High organic matter contents inhibit crystallisation or even formation of iron oxides, resulting in the state of Fe fulvates (McKeague, 1967). Diverse comments questioning correlation of Fep with organic-bound Fe (e.g. Birkeland et al., 1989; Parfitt and Childs, 1988) cannot be supported by our research. Moreover, Fep correlates positively with moisture parameters and particularly with SM, whereas no significant relations to temperature variables are evident. Importantly, SM was found being the major parameter influencing TOC contents (Baumann et al., 2009) as well as soil respiration (Geng et al., 2012) positively on the Tibetan Plateau, closing the line of argument. The opposite trend can be observed for soil acidity, with both pH and $CaCO_3$ showing a comparably high correlation (see also Shi et al., 2012). Acid soil conditions correspond to inhibited turnover of organic matter and the involved formation of fulvic acids as well as humic acids (Scheffer et al., 2002). Furthermore, the latter indirectly suggests a stable soil forming environment with little aeolian sediment input. The contrary situation can be frequently observed at sites with degrading permafrost (Yan et al., 2009). Fresh sediments are usually rich in carbonates inducing alkaline conditions with very low TOC contents (Baumann et al., 2009). Texture variables are only weakly correlated. Sand has a negative impact on Fep contents, because of its low water holding capacity and excessive drainage. As explained for the relationships of Fep with SM and TOC, this disfavours the accumulation of soil organic matter and its biochemical transformation. Moreover, this supports the above-stated relations to aeolian sedimentation processes, although the corresponding sediments consist besides fine sands also of silty material (cf. electronic supplementary data S2).

Relationships between POR are high, while Fep reveals only low correlations to POR and none to Fed/Fet. It is crucial for the interpretation of Fep as an indicator of pedogenesis without being proportional to Fet, that Fep as the only PO-fraction shows no significant correlations with Fet (Table 3). Consequently, Fep results can be fully used for statistical analyses and models without taking the relation to Fet into account. Contrarily, Fed has a strong significant correlation with Fet, which renders the evaluation of POR using Fed without reference to Fet extremely vague or impossible. Interestingly, correlation of Fep with (Fed-Feo)/Fet is negative and for Feo/Fed positive. This supports the findings, that high Fep contents are closely linked to less developed soils mainly associated with permafrost or ground water influence. It is crucial to note that the above-explained relationships between Fep, SM and TOC in topsoils account for this link. On the other side, particularly in Gleysols, deeper soil horizons frequently show reductive conditions leading to minimal Fep contents because Fep measures the amount of Fe^{3+} being complexed with organic acids.

Correlations between PO and WI are low, but generally fit well to the specific characteristics of the indices. Only CPA and FENG can be significantly related to (Fed-Feo)/Fet, albeit with low correlation values. PI shows the strongest correlation with Fed/Fet, indicating similar trends in iron release. Melke (2007) found similar results in tundra soils of Spitsbergen. Otherwise, Fet-Fed correlates best with all WI except PI. This difference expresses the silicate bound iron in relation to the complete iron (Torrent and Cabedo, 1986), which of course exhibits the closest causal relation to WI. No reliable significant correlation to WI could be found for Fep, underlining the different pathways of Fep and general weathering processes. Whereas Fed-Feo describes geochemical processes with the formation of crystalline Fe oxides, Fep illustrates a biochemical process.

3.2.2. Differences between sampling groups

Table 5 displays the significant different sampling groups as a result of two-tailed t-tests with $p < 0.05$. Based on the correlation analyses, the two POR (Fed-Feo)/Fet and Fed/Fet as well as Fep were selected to investigate the dissimilarity between the sampling groups. With regard to POR, significant differences were found for transects and main sites. SG show comparable results, except that CM and PF were solely tested significantly different for (Fed-Feo)/Fet. Other differences were always found related to PF and GL, which are frequently influenced by redoximorphic processes, thus making the interpretation for POR difficult (Blume and Schwertmann, 1969; Fiedler and Sommer, 2004). The most important outcome, however, is the clear differentiation of PF and GL for both (Fed-Feo)/Fet and Fed/Fet. This suggests considerably distinct redoxi-morphic and soil forming processes for these two SG specifically describable by PO.

As shown above, WI indicate differences between SG only by involvement of RG, whereas POR differentiate more SG clearly. WI describe the state of weathering regardless of Fe-oxides, which in turn are a very important product of soil formation processes (Kämpf et al., 2011). Consequently, POR reflect pedogenic processes much better and more in detail. To summarise, beside general limitations for the pedogenic interpretation of redoxi-morphic sites, the results are reasonable and fit well to the expected interrelations and can therefore be considered as estimations or trends.

Fep indicates a significant dissimilarity of the main sites HUA and WUD, albeit as the only PO not for EAST and WEST. Since Fep is strongly related to TOC, only SG are different, which differ greatly in TOC contents (cf. Table 2). GL and particularly PF account for the highest contents of TOC in the topsoil (Baumann et al., 2009) and hence are too similar.

3.2.3. Multiple linear regression model (MLR)

To account for the interrelationships as well as for the explanation capacity by combining different predictor variables, we used a multiple linear regression analysis. As independent variables we used MAT, MAP, $CaCO_3$, pH, as well as sand, silt, and clay contents. A MLR was conducted for each of the different sampling groups (TOTAL, EAST, WEST, HUA, WUD, RG, CM, GL, PF) to describe the effects on the dependent variables (POR) based on different meaningful stratification levels. Only models tested significant ($p < 0.05$) were used for evaluation and interpretation (Table 7).

3.2.3.1. TOTAL sampling group. Based on the entire dataset ($n = 82$) the (Fed-Feo)/Fet ratio provides the best and most reasonable result with 64% explained variance. This confirms the findings of Arduino et al. (1984) and Wagner (2005), who described this POR most useful for the estimation of the relative pedogenic age and weathering differentiation of geomorphological units. This ratio was found to be independent of varying total iron contents and general lithology, whereas Feo is low in well-weathered and high in slightly weathered samples, with Fed responding vice versa (Arduino et al., 1984). Accordingly, (Fed-Feo)/Fet parallels different weathering intensities. Moisture parameters and soil acidity are overall the most important independent parameters. Directions of the variable's effects are negative for (Fed-Feo)/Fet and Fed/Fet, however positive for Feo/Fed. Weathering intensity and iron release are lower with higher SM (cf. GL and PF sites) and pH or $CaCO_3$ contents (cf. RG sites). Very high SM values or water saturation reduce or even stop related weathering processes leading to pronounced redistribution of PO within the soil with preferential accumulation of Fed in well-aerated horizons (Blume and Schwertmann, 1969), while Fed being lowest in poorly drained soils and horizons (Fiedler and Sommer,

Table 7
Summary of the multiple linear regression model (MLR). The level of significance is marked (***p < 0.001; **p < 0.01; *p < 0.05; others p > 0.05). Directions of influence are indicated by [+] for positive and [−] for negative effects of the variable on the MLR.

	POR	Variables—ranked by significance	R^2	R^2 adj.	Significance
TOTAL	Fed/Fet	MAP*** [−], pH*** [−], SM** [−], Silt* [−], Clay [+], MAT [−]	0.55	0.51	***
	(Fed-Feo)/Fet	MAP*** [−], SM*** [−], pH*** [−], MAT [−], Silt [−], Clay [+]	0.64	0.62	***
	Feo/Fed	SM*** [+], MAP*** [+], pH* [+], Silt [+], MAT [+], Clay [−]	0.49	0.45	***
	Fep	pH*** [−], SM*** [+], Sand* [+], Clay [+], MAP [+], MAT [+]	0.63	0.60	***
	Fet-Fed	MAP*** [+], pH*** [+], Sand*** [−], MAT [+], Clay [+], SM [−]	0.50	0.46	***
	Fed-Feo	SM*** [−], MAP*** [−], Clay* [+], pH* [−], Silt [+], MAT [+]	0.59	0.55	***
EAST	Fed/Fet	pH*** [−], SM [−], Clay [−], Sand [+]	0.41	0.32	**
	(Fed-Feo)/Fet	pH** [−], SM** [−], Clay [−], Silt [+]	0.44	0.36	**
	Feo/Fed	SM* [+], MAT [+], Silt [+], Clay [+]	0.35	0.26	*
	Fep	pH*** [−], SM [+], Clay [−], Silt [+]	0.75	0.71	***
	Fed-Feo	pH** [−], SM** [−], Clay [−], Silt [−]	0.42	0.33	**
WEST	Fed/Fet	MAT*** [−], $CaCO_3$* [−], Clay* [+], SM* [−], pH [+], Sand [+], MAP [+]	0.42	0.33	***
	(Fed-Feo)/Fet	SM*** [−], MAT*** [−], pH [+], Clay [+], Sand [−], $CaCO_3$ [−], MAP [+]	0.65	0.59	***
	Feo/Fed	SM*** [+], Sand** [+], MAT** [+], $CaCO_3$ [−], pH [−], Clay [+], MAP [+]	0.70	0.65	***
	Fep	SM*** [+], Clay* [+], pH [−], Sand [+], MAP [+], MAT [−], $CaCO_3$[−]	0.67	0.62	***
	Fet-Fed	Sand*** [−], MAT*** [+], SM*** [−], pH [+], $CaCO_3$ [−], MAP [−], Clay [−]	0.85	0.83	***
	Fed-Feo	SM*** [−], Sand*** [−], pH [+], $CaCO_3$ [−], MAT [−], Clay [+], MAP [−]	0.61	0.54	***
HUA	Fed/Fet	$CaCO_3$** [−], SM** [−], Clay [+], pH [−]	0.76	0.67	**
	(Fed-Feo)/Fet	$CaCO_3$** [−], Silt* [−], Clay [+], pH [−]	0.52	0.40	*
	Fep	SM [+], pH [−], Clay [−], $CaCO_3$ [−]	0.58	0.42	*
	Fet-Fed	Clay*** [+], Silt* [−], pH [+], $CaCO_3$ [+]	0.80	0.75	***
	Fed-Feo	$CaCO_3$** [−], Silt* [−], Clay [+], pH [+]	0.55	0.44	**
WUD	Fed/Fet	SM [−], pH [+], $CaCO_3$ [−]	0.42	0.28	$P = 0.08$
	(Fed-Feo)/Fet	SM** [−], Clay** [+], $CaCO_3$ [−]	0.90	0.85	***
	Feo/Fed	Clay* [−], SM [+], $CaCO_3$ [+]	0.72	0.59	*
	Fep	Clay* [−], $CaCO_3$ [+], SM [+]	0.64	0.48	$P = 0.06$
	Fet-Fed	Clay*** [+], $CaCO_3$ [+]	0.87	0.86	***
	Fed-Feo	Clay*** [+], SM* [−], $CaCO_3$ [−]	0.92	0.89	***
CM	Fed/Fet	pH* [−], MAP [−], Sand [+], SM [−]	0.55	0.43	*
	(Fed-Feo)/Fet	pH [−], MAP [+], Sand [+], SM [−]	0.46	0.31	*P = 0.06*
	Fet-Fed	Sand*** [−], pH [+], MAP [+], SM [−]	0.86	0.82	***
	Fed-Feo	Sand** [−], SM [−], MAP [−], pH [−]	0.69	0.61	**
GL	Fed/Fet	MAP*** [−], pH* [−], MAT [+], Sand [−], SM [−]	0.70	0.62	***
	(Fed-Feo)/Fet	MAP*** [−], SM** [−], MAT [+], pH [−], Sand [−]	0.72	0.65	***
	Feo/Fed	MAP** [+], SM* [+], Sand [−], MAT [−], pH [−]	0.60	0.50	**
	Fed-Feo	MAT [−], MAP [+], Silt [+], pH [+], SM [+], Clay [+]	0.67	0.59	***
PF	Fed/Fet	pH** [−], MAP** [−], MAT* [−], Clay [+], Sand [+], SM [+]	0.52	0.38	*
	(Fed-Feo)/Fet	MAP** [−], MAT* [−], pH [−], Clay [+], SM [−], Sand [−]	0.59	0.46	**
	Feo/Fed	MAP [+], SM [+], Sand [+], MAT [+], Clay [+], pH [+]	0.59	0.46	**
	Fep	$CaCO_3$*** [−], SM [+], Clay [+], Sand [−], MAT [+]	0.72	0.65	***
	Fet-Fed	pH*** [+], MAP*** [+], Sand [−], Clay [+], MAT [+], SM [+]	0.66	0.56	***
	Fed-Feo	MAP* [−], MAT [−], Clay [+], Sand [−], pH [−], SM [−]	0.55	0.41	**

2004). Alkaline soil conditions inhibit feldspar weathering, iron release and thus the formation of clay minerals (Brady and Weil, 2008; Schwertmann, 1964). This is explicable by the buffer for silicate weathering and related iron release (Nesbitt et al., 1996). Respectively, soil acidity has the highest impact on Fed/Fet. Regarding texture parameters, silt and clay are mostly included into the models. Whereas higher clay contents indicate increased weathering and iron release, silt has the opposite influence in the MLR. PO commonly have a strong correlation to the clay content (McFadden and Hendricks, 1985) with high Feo and Fed values in the clay fraction, whereas Fet is texture-independent (Arduino et al., 1984). However, increased clay contents do not necessarily indicate higher in-situ weathering intensities, but can also be attributed to higher clay contents of substrates. Comparably strong chemical bond of PO and clay minerals can lead to enhanced PO contents even though overall weathering is low (McFadden and Hendricks, 1985; Schlichting and Blume, 1962; Torrent et al., 1980). Nevertheless, clayey substrates as the basis for soil formation as well as pedogenic translocation of clay within soils are mostly uncommon on the central-eastern Tibetan Plateau. Contrarily, high silt contents, especially in topsoils, frequently indicate comparably fresh aeolian sediments (Feng et al., 2011; Schlütz and Lehmkuhl, 2009). As Feo/Fed is an expression of recent weathering activity (Schwertmann, 1964), immature and particularly redoxi-morphic soils lead to a higher Feo/Fed ratio. Consequently, moisture variables are even more dominant: higher SM leads to less developed soils and consequently to soil horizons with a high degree of recent pedogenic activity showing high contents of oxalate-extractable oxides (Schwertmann, 1964). Although being fully aware of the unreliability and instability of PO results of redoxi-morphic soils (Blume and Schwertmann, 1969; Fiedler and Sommer, 2004), the high number and diversity of samples provide a useful overall trend as well as an indication about recent pedogenetic processes. Climate parameters (MAP and MAT) are more difficult to interpret, as particularly MAT frequently indirectly reflects and describes site-specific differences (cf. discussion about correlation of WI in Section 3.1.4).

Albeit PO-differences are difficult to interpret without being related to Fet contents and thus only giving redundant information, they can be applied to cross-validate PO ratios and particularly to verify the directions of influence (e.g. of soil acidity). Moreover, good correspondence between Fed-Feo and (Fed-Feo)/Fet gives indirect evidence that—general parameters are to be similar—also PO-differences or POR without direct relation to Fet may provide reasonable results and can be discussed pedogenetically for the respective subsample set.

Variation of Fep can be explained with the included parameters by 63%. Soil acidity is most important, followed by SM; both closely linked to TOC (cf. correlation analyses Table 3). Soils with fresh aeolian sedimentation have low soil organic matter and high carbonate contents; the latter is the specific reason for the link between pH and soil organic matter in the research area. Generally, high organic matter contents hamper crystallisation of mineral surfaces of amorphous ferric hydroxides (Schwertmann, 1966) thus leading to higher Feo and Fep contents.

As shown above, Fep can interpreted without relation to Fet contents, because it is mainly linked to organic matter.

3.2.3.2. EAST/WEST sampling group. EAST (n = 32) has the higher p-values and greater differences between multiple R^2 and corrected R^2 for all POR, which indicates a lower explanation level than for WEST (n = 50) or TOTAL. Moisture parameters and soil acidity calculate comparably to TOTAL, whereas for texture, the extreme site E2 with its high contents of partly pre-weathered and redeposited silty–sandy material is responsible for biases as well as for the vice versa influencing direction of clay (cf. Section 2.1). Overall, weathering intensities are lower for EAST compared to some western sites located around Nagqu (cf. Cambisols in W6/W7), where iron release and clay formation is higher and more noticeable in regression analyses. Additionally, the climate conditions of all four sites of EAST are rather similar, whereas distinct climate differences are evident along the western transect. Therefore, climate parameters are not included into the MLR for EAST. Altogether, WEST shows the greater explained variances and highly significant results, with SM being more dominant than for EAST.

However, MAT and some acidity parameters show opposite directions than expected for WEST, which can be related to a much broader variety of lithogenic background for the different sites (cf. ternary diagrams, Fig. 3a). Consequently, these results for WEST have to be interpreted with care, particularly for ratios without relation to Fet. Nevertheless, for both subsamples, the main outcomes fit well into the general context.

As described for TOTAL, Fe-differences are not interpretable without relation to Fet. This can be demonstrated by Fet-Fed (silicate-bound iron). The MLR is highly significant for WEST but not for EAST, which is caused by higher differences of silicate-bound iron between sites in WEST (cf. ternary diagrams indicate inhomogeneity, Fig. 3a).

Fep displays very low p-values and differences between multiple R^2 and corrected R^2. Soil acidity is dominant for EAST, whereas SM is the most important parameter for WEST. The higher explained variance for EAST is due to the more pronounced small-scale variability of SM and TOC as a result of discontinuous permafrost conditions.

To summarise, settings of EAST are climatically and geologically more homogenous. However, small-scale spatial variability of SM conditions is higher in discontinuous permafrost (cf. Zhang et al., 2003). There are more extreme sites in EAST (Table 2); e.g. being either very moist or dry with relatively fresh sedimentary layers. Overall, the environment in discontinuous permafrost areas is more unstable than in continuous permafrost. Other parameters, such as geomorphological relief position, vegetative cover and slope or geomorphologic activities like sedimentation by wind and water overprint the direct effects of SM (Wang et al., 2010; Zhang et al., 2003).

3.2.3.3. HUA/WUD sampling group. The WUD group (n = 21) has the highest explained variance for (Fed-Feo)/Fet with 85% ($p < 0.001$) of all sampling groups and corresponding dependent variables. SM has the highest influence equally followed by clay and soil acidity. Contrarily, even though mean and variance of SM are much higher (Table 3), moisture parameters are not included in HUA (n = 22). In contrast, soil acidity and texture having a dominant influence, leading to the assumption that moisture conditions are overly uniform in HUA and differences in texture/sediment composition are more prominent within the model. The latter could be also linked to the zone of discontinuous permafrost with recently more active sedimentary processes. For Feo/Fed, the same parameters as for (Fed-Feo)/Fet are selected for both sites with exactly vice versa directions of influence in the MLR. This is confirming homogenous substrate and parent material for both main sites HUA and WUD (cf. Table 2), because Feo/Fed is calculated without reference to Fet (cf. Section 3.2.1). Accordingly, ratios without relation to Fet can be evaluated likewise for each of the main sites. However, the model for HUA calculates slightly insignificant ($p = 0.08$) and also the significance for WUD is much higher for Feo/Fed ($p = 0.03$) than for (Fed-Feo)/Fet ($p = 0.0008$). Thus it can be said, that the degree of activity (Feo/Fed after Schwertmann, 1964) acts very indifferent and unstable for both sites. For Fed/Fet, HUA has the lower p-value and higher R^2, whereas WUD plots above the significance level. Hence, the degree of iron release varies more in HUA, which can be related to discontinuous permafrost and more complex sedimentary layers and processes.

This situation can also be observed and discussed for PO-differences. Much lower p-values than for POR and very high prediction accuracies ($R^2 = 0.89$ for WUD, $R^2 = 0.44$ for HUA) can be observed for Fed-Feo. Thus, the portion of well-crystallised iron oxides causes the main difference in the performance of (Fed-Feo)/Fet and Fed/Fet (Arduino et al., 1984). The variation of Feo and Fed is obviously lower in WUD, which can be observed for HUA vice versa (Table 2, variance and standard deviation). Together with the lower mean Feo and Fed contents of WUD, this provides more stable conditions for the MLR and less active weathering processes (Figs. 2 and 3). For Fet-Fed, p-values are very low with high R^2, implying that silicate bound iron can be precisely described by only few parameters. Grain size parameters and in particular clay content contribute the most to the models. Higher clay content leads to a larger ΔFet/Fed with increasing Fet contents but consistent Fed values. As described above, lower soil acidity also leads to a higher difference between Fet and Fed contents. Fed is appropriately linked to lower pH-values or $CaCO_3$ contents. Clay and $CaCO_3$ explain 86% of the variation for WUD. These very solid results are helpful to interpret other more inhomogeneous sampling groups correspondingly.

Fep only indicates multiple regressions with p-values around 0.05. The variation within sites is obviously not high enough, but results of MLR fit well into context (Table 7). Especially WUD is rather uniform concerning to TOC and SM contents (Table 2), thus including other variables into the model.

3.2.3.4. SG sampling groups. Since for SG soil profiles from different sites and transects are grouped together, the environments for soil formation and weathering are not uniform across sites. Notably, bedrock and substrates differ quite considerably (Fig. 3). This hampers the possibility of interpretation for ratios without relation to Fet and allows only inferring rough trends and estimations. Additionally, the sample set size for MLR analyses is very low in some groups (e.g. RG and CM) making results partly not evaluable. (Fed-Feo)/Fet can only be described significantly for GL and PF; CM calculates only slightly below significance level, whereas the directions indicated by the incorporated independent variables fit well into the general concept. There is a clear difference evident between GL and PF subsamples: whereas SM is a highly significant variable for GL, PF shows general site-specific climatic parameters having the highest influence. This reflects the general environments required for permafrost distribution (climate-zonal soil formation). Contrarily, GL soils are linked to a greater degree to specific geomorphological relief positions and can be found at all different climate conditions of the research area (azonal soil formation). The latter is also reflected by the lowest p-value for GL, indicating that direct influencing variables have a much higher impact for this sampling group. Weathering and activities related to pedogenic oxides are higher in GL because these soils also occur under warmer and moister climate conditions. Accordingly, more intense common soil forming and redoximorphic processes are evident, which are weakened at PF sites. Cambisol dynamics can be well demonstrated by Fed/Fet. Both the included parameters and the directions of influences are in close relation to relevant soil forming processes in Cambisols. The difference between GL and PF is also evident for this ratio. Generally, interpretation of GL is very difficult because of the complex and fast-changing processes within and between the different iron oxide fractions (see Section 3.2.2).

In terms of Fet-Fed, CM shows the highest significance followed by PF (both $p < 0.001$), whereas GL does not reveal a significant model ($p > 0.05$). Silicate-bound iron is linked to CM and PF since a higher dynamic can be found in these groups: small-scale pattern of fresh (frequently airborne) sediments and chemically weathered material.

Most importantly, only PF is significant on a very high level for Fep. Soil acidity and SM are the dominant parameters influencing the MLR in the expected directions. Lower pH means higher Fep contents (cf. strong relationship to TOC). As for GL no significant MLR could be detected, PF and GL soil groups can be considered to feature different preconditions for Fep formation and preservation. Apparently, accumulated organic matter triggered by frequent water saturation inhere other particular properties than that caused by frigid conditions. As outlined in Section 2.6, soils of PF group do not necessarily have gleyic properties. It can be thus assumed that specific redoxi-morphic as well as soil formation processes and dynamics with corresponding organic matter under the influence of permafrost are evident (Baumann et al., 2009; Dörfer et al., 2013). Further research is needed to gain closer insights regarding these particular relationships.

4. Conclusions

WI, PO fractions, and POR were successfully applied to describe distinct patterns of weathering and pedogenesis for climatic gradients along and between two north–south oriented transects across the Tibetan Plateau. WI proved to mainly indicate long-term climatically induced weathering processes. Besides weathering intensity and duration under different climate and permafrost conditions, PO and POR additionally reflect soil formation processes on a small spatial scale depending on geomorphological relief position and substrate genesis. However, at sites influenced by redox processes, Al-based WI provide more stable tools than PO for describing weathering conditions. Prevailing permafrost environments are crucial for WI and PO, showing clear differences between continuous, discontinuous, and sporadic permafrost as well as amongst degraded and non-degraded sites. This accounts particularly for the strong relationship between SM and PO ratios.

CIA proved to be the most useful and reasonable WI for assessing weathering intensities of recent soils in permafrost ecosystems, if $CaCO_3$ had been analysed in the laboratory allowing concise calculation of CaO*. According to CIA, half of all samples can be described as only slightly weathered. Almost 25% plot below or slightly above the feldspar join, emphasising the overall low weathering intensities. Nevertheless, the two main sites HUA and WUD can be explicitly differentiated in terms of parent material and climate conditions by CIA. Moreover, climate trends and permafrost conditions along transects EAST and WEST can be highlighted (cf. Fig. 3).

For POR, (Fed-Feo)/Fet provides the best results with 64% explained variation by the MLR for TOTAL sampling group, showing lower weathering intensities and iron release associated with higher SM and pH values. Another important finding is the clear differentiability between Gleysols and permafrost-affected soils, and thus among distinct redoxi-morphic and soil forming processes specifically describable by PO. Whereas SM is most important in the MLR analysis for Gleysols, permafrost-affected soils rather reflect general site-specific climatic parameters (zonal pedogenesis). Thus, Gleysols are linked to a greater extend to particular geomorphological relief positions and can be basically found under all climate conditions of the research area (azonal pedogenesis). It could be demonstrated that pyrophosphate extracts mainly organically bound pedogenic iron indicated by the high correlation to TOC ($r = 0.89$). Fep correlates highly positively with SM, whereas no significant relations to temperature variables are evident. Correlation of Fep with (Fed-Feo)/Fet is negative and for Feo/Fed positive, supporting our findings that high Fep contents are closely linked to less developed and weathered soils, mainly associated with permafrost or ground water influence. Most importantly, permafrost-affected soils are the only soil group showing a highly significant MLR for Fep. It is an essential outcome, that Gleysols do not exhibit a significant MLR, thus revealing differences compared to permafrost-affected soils, even though both typically have considerably high SM and TOC contents. It is crucial for a pedogenic interpretation that Fep shows no significant correlations with Fet, thus Fep can be fully included into statistical analyses and models without relation to Fet.

For many profiles, notably in discontinuous permafrost, distinct lower weathering intensities can be observed for the top horizons compared to the subsoil. Beside the disconnection of turf-like topsoils from the mineral soil body, this also reflects a recent input of aeolian sediments, mainly derived from proximal source areas with related permafrost degradation processes. These processes have led to the multilayered soil profiles predominating in the research area. Small-scale variability, particularly of SM conditions, is higher in discontinuous permafrost areas (EAST). Overall, the environment in discontinuous permafrost areas is more unstable and other parameters, such as relief position and slope or geomorphologic processes like sedimentation by wind and water are more important overprinting the direct effect of SM on weathering and pedogenesis.

To summarise, WI and POR provide promising tools to depict and evaluate both recent and past phases of instability and permafrost degradation processes, amplified by interrelated feedback mechanisms between global change and human activities over the past decades.

Supplementary data to this article can be found online at http://dx.doi.org/10.1016/j.geoderma.2014.02.019.

Acknowledgements

The authors would like to thank members of the Peking University expedition team and particularly Wang Liang, Yang Kuo, Mou Shanmin, Qi Shanxue, Yang Xiaoxia and Mi Zhaorong for accompanying the field work. This research was supported by the National Natural Science Foundation of China (NSFC Grants 31025005 and 31270481 to JSH) and a graduation fellowship from the state of Baden-Württemberg, Germany (Grant No. VI 4.2—661 7631.2/Baumann). We thank Sabine Flaiz, Christian Wolf and Katrin Drechsel for assistance with the laboratory works and Dr. Heinrich Taubald for X-ray fluorescence analyses.

References

Alexander, E.B., 1985. Estimating relative ages from iron-oxide/total-iron ratios of soils in the Western Po Valley, Italy—a discussion. Geoderma 35, 257–259.
An, Z., Kutzbach, J.E., Prell, W.L., Porter, S.C., 2001. Evolution of Asian monsoons and phased uplift of the Himalaya-Tibetan Plateau since Late Miocene times. Nature 411, 62–66.
Aniku, J.R., Singer, M.J., 1990. Pedogenic iron oxide trends in a marine terrace chronosequence. Soil Sci. Soc. Am. J. 54, 147–152.
Arduino, E., Barberis, E., Carraro, F., Forno, M.G., 1984. Estimating relative ages from iron-oxide/total-iron ratios of soils in the western Po Valley, Italy. Geoderma 33, 39–52.
Bascomb, C., 1968. Distribution of pyrophosphate-extractable iron and organic carbon in soils of various groups. Eur. J. Soil Sci. 19 (2), 251–268.
Baumann, F., He, J.-S., Schmidt, K., Kühn, P., Scholten, T., 2009. Pedogenesis, permafrost, and soil moisture as controlling factors for soil nitrogen and carbon contents across the Tibetan Plateau. Glob. Chang. Biol. 15 (12), 3001–3017. http://dx.doi.org/10.1111/j.1365-2486.2009.01953.x.
Bäumler, R., 2001. Pedogenic studies in aeolian deposits in the high mountain area of eastern Nepal. Quat. Int. 76 (77), 93–102.
Bäumler, R., Zech, W., 2000. Quaternary paleosols, tephra deposits and landscape history in South Kamchatka, Russia. Catena 41, 199–215.
Birkeland, P.W., Burke, R.M., Benedict, J.B., 1989. Pedogenic gradients for iron and aluminium accumulation and phosphorus depletion in arctic and alpine soils as a function of time and climate. Quat. Res. 32, 193–204.
Blume, H.P., Schwertmann, U., 1969. Genetic evaluation of profile distribution of aluminium, iron, and manganese oxides. Soil Sci. Soc. Am. Proc. 33, 438–444.
Brady, N.C., Weil, R.R., 2008. 14th ed. The Nature and Properties of Soils, xiv. Pearson Prentice Hall, Upper Saddle River, N.J. 965.
Buero, V., Schwertmann, U., 1987. Occurance and transformations of iron and manganese in a colluvial Terra Rossa toposequence of Northern Italy. Catena 14, 519–531.
Buggle, B., Glaser, B., Zöller, L., Hambach, U., Marković, S., Glaser, I., Gerasimenko, N., 2008. Geochemical characterization and origin of Southeastern and Eastern European loesses (Serbia, Romania, Ukraine). Quat. Sci. Rev. 27 (9–10), 1058–1075. http://dx.doi.org/10.1016/j.quascirev.2008.01.018.
Buggle, B., Glaser, B., Hambach, U., Gerasimenko, N., Marković, S., 2011. An evaluation of geochemical weathering indices in loess–paleosol studies. Quat. Int. 240 (1–2), 12–21. http://dx.doi.org/10.1016/j.quaint.2010.07.019.
Chapin III, F.S., Zavaleta, E.S., Eviner, V.T., Naylor, R.L., Vitousek, P.M., Reynolds, H.L., Hooper, D.U., Lavorel, S., Sala, O.E., Hobbie, S.E., Mack, M.C., Díaz, S., 2000. Consequences of changing biodiversity. Nature 405 (6783), 234–242. http://dx.doi.org/10.1038/35012241.

Cheng, G., 2005. Permafrost studies in the Qinghai–Tibet Plateau for road construction. J. Cold Reg. Eng. 19 (1), 19–29. http://dx.doi.org/10.1061/(ASCE)0887-381X(2005)19:1(19).
Cheng, G., Wu, T., 2007. Responses of permafrost to climate change and their environmental significance, Qinghai–Tibet Plateau. J. Geophys. Res. 112 (F2). http://dx.doi.org/10.1029/2006JF000631.
Cullers, R.L., 2000. The geochemistry of shales, siltstones and sandstones of Pennsylvanian–Permian age, Colorado, USA: implications for provenance and metamorphic studies. Lithos 51, 181–203.
Dahms, D., Favilli, F., Krebs, R., Egli, M., 2012. Soil weathering and accumulation rates of oxalate-extractable phases derived from alpine chronosequences of up to 1 Ma in age. Geomorphology 151–152, 99–113. http://dx.doi.org/10.1016/j.geomorph.2012.01.021.
Dai, F., Su, Z., Liu, S., Liu, G., 2011. Temporal variation of soil organic matter content and potential determinants in Tibet, China. Catena 85 (3), 288–294. http://dx.doi.org/10.1016/j.catena.2011.01.015.
Diaz, M.T.J., 1989. Mineralogy of iron oxides in two soil chronosequences of central Spain. Catena 16, 291–299.
Dietze, E., Hartmann, K., Diekmann, B., IJmker, J., Lehmkuhl, F., Opitz, S., Stauch, G., Wünnemann, B., Borchers, A., 2012. An end-member algorithm for deciphering modern detrital processes from lake sediments of Lake Donggi Cona, NE Tibetan Plateau, China. Sediment. Geol. 243–244, 169–180. http://dx.doi.org/10.1016/j.sedgeo.2011.09.014.
Domrös, M., Peng, G., 1988. The Climate of China. Springer, Berlin, Heidelberg, NewYork.
Dörfer, C., Kühn, P., Baumann, F., He, J.-S., Scholten, T., Slomp, C.P., 2013. Soil organic carbon pools and stocks in permafrost-affected soils on the Tibetan Plateau. PLoS ONE 8 (2), e57024. http://dx.doi.org/10.1371/journal.pone.0057024.
Duzgoren-Aydin, N., Aydin, A., Malpas, J., 2002. Re-assessment of chemical weathering indices: case study on pyroclastic rocks of Hong Kong. Eng. Geol. 63, 99–119.
Fang, J., Piao, S., Tang, Z., Peng, C., Ji, W., 2001. Interannual variability in net primary production and precipitation. Science 293 (5536), 1723a. http://dx.doi.org/10.1126/science.293.5536.1723a.
FAO, 2006. Guidlines for Soil Description, 4th edn. (Rome, 98 pp.).
Fedo, C.M., Nesbitt, W.H., Young, G.M., 1995. Unraveling the effects of potassium metasomatism in sedimentary rocks and paleosols, with implications for paleoweathering conditions and provenance. Geology 23 (10), 921. http://dx.doi.org/10.1130/0091-7613(1995)023<0921:UTEOPM>2.3.CO;2.
Feng, Z.-D., 1997. Geochemical characteristics of a loess-soil sequence in central Kansas. Soil Sci. Soc. Am. J. 61, 534–541.
Feng, J.-L., Zhu, L.-P., 2009. Origin of terra rossa on Amdo North Mountain on the Tibetan Plateau, China: evidence from quartz. Soil Sci. Plant Nutr. 55 (3), 407–420. http://dx.doi.org/10.1111/j.1747-0765.2009.00370.x.
Feng, J.-L., Hu, Z.-G., Ju, J.-T., Zhu, L.-P., 2011. Variations in trace element (including rare earth element) concentrations with grain sizes in loess and their implications for tracing the provenance of eolian deposits. Quat. Int. 236 (1–2), 116–126. http://dx.doi.org/10.1016/j.quaint.2010.04.024.
Fiedler, S., Sommer, M., 2004. Water and redox conditions in wetland soils—their influence on pedogenic oxides and morphology. Soil Sci. Soc. Am. J. 68, 326–335.
Gallet, S., Jahn, B., van Vliet Lanoe, B., Dia, A., Rossello, E., 1998. Loess geochemistry and its implications for particle origin and composition of the upper continental crust. Earth Planet. Sci. Lett. 156, 157–172.
Gao, Q., Li, Y., Wan, Y., Lin, E., Xiong, W., Jiangcun, W., Wang, B., Li, W., 2006. Grassland degradation in Northern Tibet based on remote sensing data. J. Geogr. Sci. 16 (2), 165–173. http://dx.doi.org/10.1007/s11442-006-0204-1.
Geng, Y., Wang, Y., Yang, K., Wang, S., Zeng, H., Baumann, F., Kuehn, P., Scholten, T., He, J.-S., Bond-Lamberty, B., 2012. Soil respiration in Tibetan alpine grasslands: belowground biomass and soil moisture, but not soil temperature, best explain the large-scale patterns. PLoS ONE 7 (4), e34968. http://dx.doi.org/10.1371/journal.pone.0034968.
Gruber, S., 2012. Derivation and analysis of a high-resolution estimate of global permafrost zonation. The Cryosphere 6 (1), 221–233.
Harnois, L., 1988. The CIW index: a new chemical index of weathering. Sediment. Geol. 55, 319–322.
He, J.-S., Wang, Z., Wang, X., Schmid, B., Zuo, W., Zhou, M., Zheng, C., Wang, M., Fang, J., 2006. A test of the generality of leaf trait relationships on the Tibetan Plateau. New Phytol. 170 (4), 835–848. http://dx.doi.org/10.1111/j.1469-8137.2006.01704.x.
He, J.-S., Wang, X., Flynn, D.F.B., Wang, L., Schmid, B., Fang, J., 2009. Taxonomic, phylogenetic, and environmental trade-offs between leaf productivity and persistence. Ecology 90 (10), 2779–2791. http://dx.doi.org/10.1890/08-1126.1.
Hu, H., Wang, G., Liu, G., Li, T., Ren, D., Wang, Y., Cheng, H., Wang, J., 2009. Influences of alpine ecosystem degradation on soil temperature in the freezing–thawing process on Qinghai–Tibet Plateau. Environ. Geol. 57 (6), 1391–1397. http://dx.doi.org/10.1007/s00254-008-1417-7.
IUSS Working Group, 2006. World reference base for soil resources. World Soil Resources Reports, 103.
Jenny, H., 1994. Factors of Soil Formation: A system of Quantitative Pedology, xviii. Dover, New York 281.
Jin, H., Li, S., Cheng, G., Shaoling, W., Li, X., 2000. Permafrost and climatic change in China. Glob. Planet. Chang. 26, 387–404.
Kaiser, K., 2004. Pedogeomorphological transect studies in Tibet: implications for landscape history and present-day dynamics. Pr. Geograficzne 200, 147–165.
Kaiser, K., Schoch, W.H., Miehe, G., 2007. Holocene paleosols and colluvial sediments in Northeast Tibet (Qinghai Province, China): properties, dating and paleoenvironmental implications. Catena 69 (2), 91–102. http://dx.doi.org/10.1016/j.catena.2006.04.028.
Kaiser, K., Miehe, G., Barthelmes, A., Ehrmann, O., Scharf, A., Schult, M., Schlütz, F., Adamczyk, S., Frenzel, B., 2008. Turf-bearing topsoils on the central Tibetan Plateau, China: pedology, botany, geochronology. Catena 73 (3), 300–311. http://dx.doi.org/10.1016/j.catena.2007.12.001.
Kämpf, N., Scheinost, A.C., Schulze, D.G., 2011. Oxide minerals. In: Huang, P., Li, Y., Sumner, M.E. (Eds.), Handbook of Soil Science, Properties and Processes. Part III: Soil Mineralogy. CRC Press, pp. 125–168.
Kang, S., Xu, Y., You, Q., Flügel, W.-A., Pepin, N., Yao, T., 2010. Review of climate and cryospheric change in the Tibetan Plateau. Environ. Res. Lett. 5 (1), 15101. http://dx.doi.org/10.1088/1748-9326/5/1/015101.
Cryosols. Permafrost-Affected Soils. In: Kimble, J. (Ed.), Springer, Berlin.
Kronberg, B., Nesbitt, H.W., 1981. Quantification of weathering, soil geochemistry and soil fertility. Eur. J. Soil Sci. 32, 453–459.
Kühn, P., Techmer, A., Weidenfeller, M., 2013. Lower to middle Weichselian pedogenesis and palaeoclimate in Central Europe using combined micromorphology and geochemistry: the loess–paleosol sequence of Alsheim (Mainz Basin, Germany). Quat. Sci. Rev. 75, 43–58. http://dx.doi.org/10.1016/j.quascirev.2013.05.019.
Mahaney, W., Fahey, B., 1980. Morphology, composition and age of a buried paleosol, Front Range, Colorado, U.S.A. Geoderma 23, 209–218.
McFadden, L.D., Hendricks, D.M., 1985. Changes in the content and composition of pedogenic iron oxyhydroxides in a chronosequence of soils in Southern California. Quat. Res. 23, 189–204.
McKeague, J.A., 1967. An evaluation of 0.1 M pyrophosohate and pyrophasphate-dithionite in comparison with oxalate as extractants of the accumulation products in podzols and some other soils. Can. J. Soil Sci. 47, 95–99.
McLennan, S.M., 1993. Weathering and global denudation. J. Geol. 101 (2), 295–303.
McLennan, S.M., 2001. Relationships between the trace element composition of sedimentary rocks and upper continental crust. Geochem. Geophys. Geosyst. 2 (4). http://dx.doi.org/10.1029/2000GC000109.
Mehra, O., Jackson, M., 1960. Iron oxide removal from soils and clays by a dithionite-citrate buffered with sodium bicarbonats. Clays Clay Miner. 7, 317–327.
Melke, J., 2007. Weathering processes in the soils of tundra of western Spitsbergen. Pol. J. Soil Sci. 40 (2), 217–226.
Mirabella, A., Carnicelli, S., 1992. Iron oxide mineralogy in red and brown soils developed on calcareous rocks in central Italy. Geoderma 55, 95–109.
Nesbitt, H.W., Young, G.M., 1982. Early Proterozoic climates and plate motions inferred from major element chemistry of lutites. Nature 299, 715–717.
Nesbitt, H.W., Young, G.M., 1984. Prediction of some weathering trends of plutonic and volcanic rocks based on thermodynamic and kinetic considerations. Geochim. Cosmochim. Acta 48, 1523–1534.
Nesbitt, H.W., Young, G.M., McLennan, S., Keays, R., 1996. Effects of chemical weathering and sorting on the petrogenesis of siliciclastic sediments, with implications for provenance studies. J. Geol. 104, 525–542.
Niu, F., Lin, Z., Liu, H., Lu, J., 2011. Characteristics of thermokarst lakes and their influence on permafrost in Qinghai–Tibet Plateau. Geomorphology 132 (3–4), 222–233. http://dx.doi.org/10.1016/j.geomorph.2011.05.011.
Parfitt, R., Childs, C., 1988. Estimation of forms of Fe and Al: a review, and analysis of contrasting soils by dissolution and Moessbauer methods. Aust. J. Soil Res. 26, 121–144.
Parker, A., 1970. An index of weathering for silicate rocks. Geol. Mag. 107, 501–504.
Ping, C.-L., Qiu, G., Zhao, L., 2004. The periglacial environment of China. In: Kimble, J. (Ed.), Cryosols. Permafrost-Affected Soils. Springer, Berlin, pp. 275–291.
Price, J.R., Velbel, M.A., 2003. Chemical weathering indices applied to weathering profiles developed on heterogeneous felsic metamorphic parent rocks. Chem. Geol. 202 (3–4), 397–416. http://dx.doi.org/10.1016/j.chemgeo.2002.11.001.
Qiu, J., 2008. China: the third pole. Nature 454 (7203), 393–396. http://dx.doi.org/10.1038/454393a.
R Development Core Team, 2012. R: ALanguage and Environment for Statistical Computing. R Foundation for Statistical Computing, Vienna, Austria.
Rezapour, S., Jafarzadeh, A.A., Samadi, A., Oustan, S., 2010. Distribution of iron oxides forms on a transect of calcareous soils, north-west of Iran. Arch. Agron. Soil Sci. 56 (2), 165–182. http://dx.doi.org/10.1080/03650340902956660.
Sauer, D., Wagner, S., Brückner, H., Scarciglia, F., Mastronuzzi, G., Stahr, K., 2010. Soil development on marine terraces near Metaponto (Gulf of Taranto, southern Italy). Quat. Int. 222 (1–2), 48–63. http://dx.doi.org/10.1016/j.quaint.2009.09.030.
Scheffer, F., Schachtschabel, P., Blume, H.-P., 2002. Lehrbuch der Bodenkunde, 15th ed. Spektrum, Akad. Verl., Heidelberg [u.a.], XIV, p. 593 S.
Schlichting, E., Blume, H.-P., 1962. Art und Ausmaß der Veränderungen des Bestandes mobiler Oxyde in Böden aus jungpleistozänem Geschiebemergel und ihren Horizonten. J. Plant Nutr. Soil Sci. 96, 144–156.
Schlütz, F., Lehmkuhl, F., 2009. Holocene climatic change and the nomadic Anthropocene in Eastern Tibet: palynological and geomorphological results from the Nianbaoyeze Mountains. Quat. Sci. Rev. 28 (15–16), 1449–1471. http://dx.doi.org/10.1016/j.quascirev.2009.01.009.
Schwertmann, U., 1964. Differenzierung der Eisenoxide des Bodens durch Extraktion mit Ammoniumoxalat-Lösung. J. Plant Nutr. Soil Sci. 105, 194–202.
Schwertmann, U., 1966. Inhibitory effect of soil organic matter on the crystallization of amorphous ferric hydroxide. Nature 212 (5062), 645–646. http://dx.doi.org/10.1038/212645b0.
Shi, Y., Baumann, F., Ma, Y., Song, C., Kühn, P., Scholten, T., He, J.-S., 2012. Organic and inorganic carbon in the topsoil of the Mongolian and Tibetan grasslands: pattern, control and implications. Biogeosciences 9 (6), 2287–2299. http://dx.doi.org/10.5194/bg-9-2287-2012.
Torrent, J., Cabedo, A., 1986. Sources of iron oxides in reddish brown soil profiles from calcarenites in southern Spain. Geoderma 37, 57–66.
Torrent, J., Schwertmann, U., Schulze, D.G., 1980. Iron oxide mineralogy of some soils of two river terrace swquences in Spain. Geoderma 23, 191–208.
Torrent, J., Liu, Q., Bloemendal, J., Barrón, V., 2007. Magnetic enhancement and iron oxides in the Upper Luochuan loess–paleosol sequence, Chinese Loess Plateau. Soil Sci. Soc. Am. J. 71 (5), 1570. http://dx.doi.org/10.2136/sssaj2006.0328.

Vitousek, P.M., 1997. Human domination of earth's ecosystems. Science 277 (5325), 494–499. http://dx.doi.org/10.1126/science.277.5325.494.

Wagner, M., 2005. Geomorphological and pedological investigations on the glacial history of the Kali Gandaki (Nepal Himalaya). GeoJournal 63 (1–4), 91–113. http://dx.doi.org/10.1007/s10708-005-2397-8.

Wang, B., French, H.M., 1994. Climate controls and high-altitude permafrost, Qinghai–Xizang (Tibet) Plateau, China. Permafr. Periglac. Process. 5 (2), 87–100. http://dx.doi.org/10.1002/ppp.3430050203.

Wang, S., Jin, H., Li, S., Zhao, L., 2000. Permafrost degradation on the Qinghai–Tibet Plateau and its environmental impacts. Permafr. Periglac. Process. 11, 43–53.

Wang, G., Liu, L., Liu, G., Hu, H., Li, T., 2010. Impacts of grassland vegetation cover on the active-layer thermal regime, northeast Qinghai–Tibet Plateau, China. Permafr. Periglac. Process. 21 (4), 335–344. http://dx.doi.org/10.1002/ppp.699.

Wang, G., Bai, W., Li, N., Hu, H., 2011. Climate changes and its impact on tundra ecosystem in Qinghai–Tibet Plateau, China. Clim. Chang. 106 (3), 463–482. http://dx.doi.org/10.1007/s10584-010-9952-0.

Xue, X., Guo, J., Han, B., Sun, Q., Liu, L., 2009. The effect of climate warming and permafrost thaw on desertification in the Qinghai–Tibetan Plateau. Geomorphology 108 (3–4), 182–190. http://dx.doi.org/10.1016/j.geomorph.2009.01.004.

Yan, C., Song, X., Zhou, Y., Duan, H., Li, S., 2009. Assessment of aeolian desertification trends from 1975's to 2005's in the watershed of the Longyangxia Reservoir in the upper reaches of China's Yellow River. Geomorphology 112 (3–4), 205–211. http://dx.doi.org/10.1016/j.geomorph.2009.06.003.

Yang, S., Jung, H.-S., Li, C., 2004. Two unique weathering regimes in the Changjiang and Huanghe drainage basins: geochemical evidence from river sediments. Sediment. Geol. 164 (1–2), 19–34. http://dx.doi.org/10.1016/j.sedgeo.2003.08.001.

Yang, Y., Fang, J., Smith, P., Tang, Y., Chen, A., Ji, C., Hu, H., Rao, S., Tan, K., He, J.-S., 2009. Changes in topsoil carbon stock in the Tibetan grasslands between the 1980s and 2004. Glob. Chang. Biol. 15 (11), 2723–2729. http://dx.doi.org/10.1111/j.1365-2486.2009.01924.x.

Yang, M., Nelson, F.E., Shiklomanov, N.I., Guo, D., Wan, G., 2010. Permafrost degradation and its environmental effects on the Tibetan Plateau: a review of recent research. Earth Sci. Rev. 103 (1–2), 31–44. http://dx.doi.org/10.1016/j.earscirev.2010.07.002.

Yang, Z., Ouyang, H., Zhang, X., Xu, X., Zhou, C., Yang, W., 2011. Spatial variability of soil moisture at typical alpine meadow and steppe sites in the Qinghai–Tibetan Plateau permafrost region. Environ. Earth Sci. 63 (3), 477–488. http://dx.doi.org/10.1007/s12665-010-0716-y.

Zhang, Y., Ohata, T., Kadota, T., 2003. Land-surface hydrological processes in the permafrost region of the eastern Tibetan Plateau. J. Hydrol. 283 (1–4), 41–56. http://dx.doi.org/10.1016/S0022-1694(03)00240-3.

Zhang, F., Wang, T., Xue, X., Han, B., Peng, F., You, Q., 2010. The response of soil CO2 efflux to desertification on alpine meadow in the Qinghai–Tibet Plateau. Environ. Earth Sci. 60 (2), 349–358. http://dx.doi.org/10.1007/s12665-009-0421-x.